Matmon, A., Fink, D., Davis, M., Niedermann, S., Rood, D., Frumkin, A. (2014): Unraveling rift margin evolution and escarpment development ages along the Dead Sea fault using cosmogenic burial ages. - *Quaternary Research*, *82*, 1, p. 281-295.

DOI: http://doi.org/10.1016/j.yqres.2014.04.008

Unraveling rift margin evolution and escarpment development ages along the Dead Sea fault using cosmogenic burial ages

Matmon, A[1]., Fink, D[2]., Davis, M[1]., Niedermann, S[3]., Rood, D[4]., Frumkin, A[5].
[1]The Institute of Earth Sciences, Hebrew University of Jerusalem, Givat Ram, Jerusalem 91904, Israel
[2] Australian Nuclear Science and Technology Organization, PMB1, Menai, NSW 2234, Australia
[3]Helmholtz-Zentrum Potsdam - Deutsches GeoForschungsZentrum, Telegrafenberg, D-14473 Potsdam, Germany
[4]Center for Accelerator Mass Spectrometry, Lawrence Livermore National Laboratory, P.O. Box 808, L-397, Livermore, CA 94550, USA
[5]Department of Geography, The Hebrew University of Jerusalem, Jerusalem 91905, Israel

Abstract

The Dead Sea fault (DSF) is one of the most active plate boundaries in the world. Understanding the Quaternary history and sediments of the DSF requires investigation into the Neogene development of this plate boundary. DSF lateral motion preceded significant extension and rift morphology by ~10 Ma. Sediments of the Sedom Formation, dated here between 5.0±0.5 Ma and $6.2^{+inf}_{-2.1}$ Ma, yielded extremely low ^{10}Be concentrations and ^{26}Al is absent. These reflect the antiquity of the sediments, deposited in the Sedom Lagoon, which evolved in a subdued landscape and was connected to the Mediterranean Sea. The base of the overlying Amora Formation, deposited in the terminal Amora Lake which developed under increasing relief that promoted escarpment incision, was dated at $3.3^{+0.9}_{-0.8}$ Ma. Burial ages of fluvial sediments within caves (3.4±0.2 Ma and 3.6±0.4 Ma) represent the timing of initial incision. Initial DSF topography coincides with the earliest Red Sea MORB's and the East Anatolian fault initiation. These suggest a change in the relative Arabian-African plate motion. This change introduced the rifting component to the DSF followed by significant subsidence, margin uplift, and a reorganization of relief and drainage pattern in the region resulting in the topographic framework observed today.

Introduction

Temporal frameworks of rift morphology initiation and formation of rift-margin escarpments are difficult to establish. Sometimes, these can be provided based on seismic stratigraphy, radiometric dating, lithostratigraphy and/or biostratigraphy (e.g. Summerfield, 1991a,b; Ollier, 1995; Rosendahl, 1987; Ebinger, 1989; Ebinger et al., 1987). One of the youngest, most active, and studied rifts in the world is located along the Dead Sea fault (DSF) which is part of the Arabian-African plate boundary. The DSF, defined geographically from the Gulf of Aqaba to the Lebanon Mountains, connects the spreading zones of the Red Sea and Gulf of Aden with the convergence belts along the northern Mediterranean Sea, Turkey, and Iran (Fig. 1). The evolution of the Arabian plate boundaries is inherently related to the way it translates relative to the African plate. As such, the DSF provides the opportunity to understand the temporal relations between tectonic activity (i.e. motion along faults) and the development of topography. To understand the present relations between tectonic activity and morphology and the way they developed throughout the Quaternary it is essential to go back several million years, describe the major phases in the tectonic activity of the DSF, and determine the time and processes that triggered major morphologic development. Specifically, the Quaternary landscape evolution of the western margin of the DSF stems from the Neogene tectonic evolution of the Dead Sea plate boundary and the Pleistocene-Holocene development of drainage systems can be understood only in the light of the preceding tectonic processes.

Sediments and Paleohydrology of the Dead Sea basin

The sediments deposited in the water bodies of the Dead Sea basin include coarse to fine clastic sediments, dolomites, and evaporates such as aragonite, gypsum, and halite (Zak, 1967; Begin et al., 1974; Ken-Tor et al., 2001a,b). These sediments reflect the environmental conditions that existed during the life span of each lake and comprise the Dead Sea Group (Zak, 1967), which includes, from oldest to most recent, the Sedom, Amora, Lisan, and Ze'elim Formations (Fig. 2). The earliest known water body in the DSF is the Sedom Lagoon, an elongated gulf connected to the Mediterranean Sea through the Yizre'el Valley (Neev and Emery, 1967; Zak, 1967) (Fig. 3). The Sedom Formation, deposited in the Sedom Lagoon, consists of a series of 1500-2000 m thick evaporites, shales, dolomites, and sand. Since the end of the Sedom lagoonal stage, the Dead Sea rift valley has been occupied by terminal lakes of which Lake Amora, Lake Lisan and the Dead Sea are the better-studied ones (Katz and Starinsky, 2009).

In the Miocene, during the initial stages of Dead Sea fault activity, extension was not significant enough to promote development of a deep rift valley with uplifted rift shoulders. The shallow valley which then existed along the Dead Sea fault accommodated intermittent lagoons that extended to the Mediterranean Sea (Katz and Starinsky, 2009). Nevertheless, in some places rivers that originated hundreds of kilometers east of the plate boundary flowed to the west and drained into the Mediterranean (Neev, 1960; Garfunkel and Horowitz, 1966; Calvo and Bartov, 2001; Calvo, 2002). Overall, the landscape and drainage systems were continuous across the Dead Sea plate boundary. The morphological barriers of the valley and the main water divide between the Dead Sea and the Mediterranean Sea did not exist at these times. At some point during the Plio-Pleistocene the scale of rift subsidence combined with uplift along the western margin was sufficient to cause collapse of the contemporary drainage pattern and create a continuous water divide between the evolving rift and the Mediterranean Sea (Picard, 1943; Garfunkel and Horowitz, 1966; Zilberman et al., 1996; Wdowinski and Zilberman, 1997; Avni et al., 2000). Drainage systems developed on both sides of this established water divide: westward-flowing streams that flowed to the Mediterranean Sea, and a system of eastward-flowing streams that incised deeply in response to significant subsidence in the Dead Sea area.

Geochronology of the Dead Sea basin

Our general understanding of the evolution of the Dead Sea fault shows that lateral motion initiated about 18 – 14 Ma (Bartov et al, 1980) but that subsequent development of rift morphology and relief formation occurred many millions of years later. Earlier studies suggest that the establishment of the present relief and drainage systems along the western margin of the DSF occurred more recently during the early Pliocene and into the Quaternary (e.g. Matmon et al., 1999, 2000; Guralnik et al., 2010). This long-scale chronology is based on regional geologic correlations (Zak, 1967; Shaliv, 1991) and few radiometric ages (Steinitz and Bartov, 1991) of basalts that limit the time of formation of presently existing canyons. During the Pliocene, increased extension along the DSF resulted in development of a deep inland drainage basin (Garfunkel, 1981). The initiation of major relief formation after millions of years of dominant lateral slip may be an expression of significant changes in the relative motion between the Arabian and African plates. Similar geomorphic processes of basin evolution have been reported from other extensional provinces around the world (e.g. Summerfield, 1991a,b; Ollier, 1995; Zelilidis, 2000; Mack et al., 2006).

Previous age estimates of the Sedom Formation range between 12 and 3 Ma, based on stratigraphical-paleogeographical and geochemical considerations (Zak, 1967; Agnon, 1983a, 1993; Shaliv, 1989; Shaliv, 1991; Steinitz and Bartov, 1991; Stein et al., 1994; Stein et al., 2000; Horowitz, 2001; Stein and Agnon, 2007; Torfstein, 2008; Ryb et al., 2009a). The fossil assemblage in the formation does not enable its dating (Zak, 1967). Current efforts using meteoric ^{10}Be concentrations in the Sedom Formation halite place it in the early to middle Pliocene (Belmaker et al., 2013).

The the Amora Formation, includes the lacustrine sequence overlying the Sedom Formation (Torfstein et al., 2009; Zak, 1967). The Amora Formation exposure at the eastern flanks of Mt. Sedom is ~300 m thick and consists of alternating aragonite–detritus laminae (Marco, 1996), halite, and clastic sediments. Age estimates based on different techniques for the Amora Formation outcrop are all <1 Ma (Zak, 1967; Kaufman, 1971; Torfstein et al., 2009). The unexposed base of the Amora Formation and the age of the Sedom-Amora contact have yet to be dated. Overall, the lithology of the Amora section is similar to that of overlying sediments comprising the Pleistocene Lake Lisan and Holocene Dead Sea (e.g. Katz and Starinsky, 2009). Based on geological considerations and field relation, Zak (1967) estimated the age of the Amora Formation to be between 1 Ma and ~100 ka. Kaufman (1971) provided three U–Th ages that range between 380 ka and 190 ka. Torfstein et al. (2009) dated the exposed upper part of the Amora Formation using the U-disequilibrium dating method to range between ~500 ka (their stratigraphically lowest sample) and ~150 ka (their stratigraphically highest sample).

The time at which the Sedom Formation ceased sedimentation and the Amora Formation started being deposited highlights a special and significant point in the morphotectonic evolution of the Dead Sea plate boundary. Until then, sedimentation in the basins competed with subsidence, Mediterranean waters could flow into the DSF valley through structural and topographic lows, and some major rivers continued flowing across the fault westward (Neev, 1960; Zilberman, 1993). From that time on, the rate of subsidence outpaced the rate of sedimentation, forcing the Dead Sea valley to become an inland endorheic basin whose base level directed river flow into it, effectively disconnecting transfer between the Mediterranean Sea and regions east of the plate boundary (Katz and Starinsky, 2009). This change set the scene for the Quaternary evolution of DSF morphology and to the establishment of the current drainage pattern along the margins of the rift. Determining when this shift occurred is needed for the overall understanding of the evolution of this major plate boundary.

Cosmogenic burial dating

The application of terrestrial cosmogenic nuclides (TCN) provides insight into the important evolutional stage in the DSF history that occurred during the Pliocene and controlled the Quaternary landscape evolution of this region. Cosmogenic radionuclides such as ^{26}Al and ^{10}Be (0.705 and 1.39 Ma half lives, respectively; Chmeleff et al., 2010; Korschinek et al., 2010; Nishiizumi, 2004) and stable ^{21}Ne are produced in-situ within minerals at the Earth's surface (e.g. Gosse and Phillips, 2001; Niedermann, 2002). After sufficient exposure, production balances loss via the sum of decay and erosion, whereby radionuclide concentrations reach a steady-state or secular equilibrium value which is effectively a function of the erosion rate (e.g. Granger, 2006):

$$N_i = P_i/[\left(\frac{1}{\tau_i}\right) + \frac{\rho\varepsilon}{\Lambda}] \quad (1)$$

where P_i is the production rate of nuclide i at the site of interest (atoms yr^{-1} g^{-1} quartz), N_i is the concentration (atoms g^{-1} quartz), τ_i is the mean life (yr), ε is the erosion rate (cm yr^{-1}), Λ is the attenuation length (g cm^{-2}), and ρ is the rock density (g cm^{-3}).

Cosmogenic burial dating employs the measurement of paired terrestrial cosmogenic nuclides in buried sedimentary quartz grains. When quartz grains that are dosed with cosmogenic nuclides are transported and buried to a sufficient depth (generally more than several tens of meters) that shields cosmic radiation, production ceases and only radioactive decay controls their concentration ratio. Thus, due to the shorter half-life of ^{26}Al compared to ^{10}Be, the ^{26}Al/^{10}Be ratio decreases as a function of burial time. The ^{26}Al/^{10}Be surface production rate ratio is 6.75 (Balco and Shuster, 2009). For most environments, the concentration ratio of ^{26}Al/^{10}Be is identical to the production rate ratio. Hence, for most cases we can assume that the initial $^{26}Al/^{10}Be$ ratio is ~6.75. It should be noted that for quartz sourced from very slow eroding terrains or extended (>1Ma) continuous exposure, the $^{26}Al/^{10}Be$ initial ratio can decrease to as low as ~ 3.45. Nevertheless, in most cases measured $^{26}Al/^{10}Be$ ratios that are lower than 6.75 suggest long periods of burial. The time dependent $^{26}Al/^{10}Be$ ratio during burial can be described by the equation (Granger et al., 1997):

$$\left(\frac{N_{26}}{N_{10}}\right)_{t_b} = \left(\frac{N_{26}}{N_{10}}\right)_0 e^{-t_{burial}\left(\frac{1}{\tau_{26}}-\frac{1}{\tau_{10}}\right)} \quad (2)$$

where $\left(\frac{N_{26}}{N_{10}}\right)_{t_b}$ is the ratio of ^{26}Al and ^{10}Be after a burial period of time t_b , $\left(N_{26}/N_{10}\right)_0$ is the initial $^{26}Al/^{10}Be$ ratio at time of burial, t_b is the time since burial, and τ_{26} and τ_{10} are the mean lives of ^{26}Al and ^{10}Be (τ_{26}=1.01±0.04 Ma and τ_{10}=2.00±0.08 Ma), respectively. Equations 1 and 2 can be solved iteratively to yield the burial age and the source erosion rate (Granger et al., 1997). The $^{21}Ne/^{10}Be$ production ratio is 4.08, and the $^{21}Ne/^{26}Al$ production ratio is 0.606 (Balco and Shuster, 2009). These ratios also change during burial since ^{21}Ne does not decay while the two other nuclides do. In this paper we use cosmogenic isotope burial dating to explore one of the major stages in the evolution of the DSF: the stage at which the rift became an inland base level disconnected from the Mediterranean and topography initiated along its margins.

We present TCN burial ages for three groups of samples: 1) samples from the top of the Sedom Formation, representing the final stages of deposition from water bodies that were connected to the Mediterranean Sea (labeled as SDM samples), 2) samples from the base of the Amora Formation, representing the initial stages of deposition from water bodies that were not connected to the Mediterranean Sea and were confined to the Dead Sea rift valley (labeled as AMZ samples), and 3) samples from two caves. The Cave of the Letters (labeled as COL samples) is close to the top of the canyon cliffs of Wadi Hever, a major canyon flowing into the Dead Sea. The Masada cave (labeled as the MZ sample) is located close to the top of the escarpment flanking the Dead Sea on the west. Buried sediments within these caves should post-date SDM samples and be similar to AMZ samples, as they represent the initial stages of relief forming and incision along the Dead Sea escarpment, that followed subsidence of the Dead Sea basin and the uplift of its western margin. In the following sections we compare burial ages using different isotopic pairs ($^{26}Al/^{10}Be$, $^{26}Al/^{21}Ne$, $^{10}Be/^{21}Ne$) and highlight the difficulties when interpreting such cosmogenic nuclide data pertaining to ancient landscapes and sediments with burial ages in the Plio-Pleistocene age range.

Site description and sampling strategy

The Sedom Formation is exposed in Mount Sedom, a rising salt diapir located within the Dead Sea rift valley along the southwestern shores of the Dead Sea, Israel (Weinberger et al., 2006) (Figs. 3,4). The diapir is rising at a rapid rate of 5-9 mm yr^{-1} (Frumkin, 2009; Pe'eri et al., 2004). Four samples (SDM 2,3,4,5; Fig. 4) were collected from a terrigenous quartz-rich sand layer, located about 250 m below the Sedom and Amora Formation boundary.

The samples were collected from a dry ravine incised ~20 m into the soft sediments. To further eliminate the interference of recent cosmogenic nuclide production, loose streambed material was removed and an additional 0.5-1 m were dug into the soft sediment before the quartz was collected. Some of the samples were dug from the base of small knickpoints (1-2 m) increasing the total overburden.

The Amiaz-1 deep borehole is located west of Mt. Sedom (Figs. 3,4) and penetrates 3.4 km of basin fill (Kashai and Croker, 1987). Three medium-coarse quartz sand samples (AMZ 1,2,3) of fluvial origin were obtained for TCN burial dating. The sampled section is attributed to the base of the Amora Formation (Kashai and Croker, 1987) and lies immediately above evaporates of the Sedom Formation. TCN burial ages of the Amiaz-1 borehole samples provide an age for the base of the Amora Formation and a minimum age constraint for the top of the Sedom Formation. Sedom Formation sand beds, such as those found in the Benot Lot member, were not available from this core.

The Cave of the Letters is located 160 m above sea level, 3 km west of the Dead Sea at the northern wall of Wadi Hever (Figs. 3,5), a deep canyon draining into the Dead Sea. The thalweg of Wadi Hever canyon lies 230 m below the Cave of the Letters and the top of the escarpment is 70 m above the cave. The Cave of the Letters is located within Turonian limestone, and cave sediments consist of autogenic dolomite, collapsed rocks and sorted fine-grained clastics (Frumkin, 2001) (Fig. 5) which are moderately bedded to laminated, with cross bedding structures. Individual sand grains are well-rounded, indicating transport by water. The cave origin is hypogene without a vadose stream, hence fluvial deposits within the cave must originate from sediments transported by Wadi Hever as it incised and truncated the pre-existing cave (Frumkin, 2001). Biogenic activity in the form of wasp drill holes (ranging in diameter from a few mm to 1 cm) is apparent in the soft sediment in the cave (Fig. 5) as well as in the exposed sediments along the wall of the canyon. Although this disturbance is recognized, we collected samples from this cave for cosmogenic burial dating. Five samples were collected, four from the top of the sedimentary column, deep within the cave passages, 10-21 m from the entrance (COL 1,2,5,7), and one from the face of exposed sediment along the external wall of the canyon (COL 3). We avoided sampling sections that showed clear evidence of wasp drilling. However, we assume that such biogenic activity has continued since the sediment was excavated to allow easier passage into the back of the cave, ~2000 yr ago, and therefore, consider all our results from the Cave of the Letters as minimum ages because the ancient buried sediment may have been mixed with modern silt.

The Masada cave is located on the main escarpment of the Dead Sea below the ruins of the archeological site of Masada (Fig. 6). The cave is located in Turonian carbonate rocks, 10 m above sea level, ~20 m below the upper desert surface and about 400 m above the Dead Sea. Similar to the COL setting, the Masada cave was exposed during the initial stages of Dead Sea escarpment formation. Shoreline sediments were washed into the cave when it was at lake level and since then have been buried within the cave and preserved from erosion. The burial age of these shoreline sediments correlates to the initial stages of Dead Sea escarpment formation. We collected one sediment sample (MZ2) from a sandy lens, composed mostly of chert fragments from the back of the cave (Fig. 6) where the sediment is well shielded from the opening of the cave entrance and its overburden is the thickest.

All samples were sieved and the 250-850 µm size fraction was further processed. Quartz was separated after carbonate dissolution in warm HCl (18%) and magnetic separation. Quartz was further etched three times in a 2.5% HF:1% HNO_3 solution. Extraction of Al and Be followed standard techniques described in Bierman and Caffee (2001). Three samples from the Sedom Formation were analyzed for $^{10}Be/^{9}Be$ and $^{26}Al/^{27}Al$ ratios at the ANTARES Accelerator Mass Spectrometry (AMS) facility at the Australian Nuclear Science and Technology Organization (ANSTO) (Fink and Smith, 2007). All other samples were analyzed at the Lawrence Livermore National Laboratory (LLNL) (Rood et al., 2010). Two Amora Formation samples (AMZ-1 and

AMZ-3) and two Cave of the Letter samples (COL-1 and COL-2) were analyzed for ^{21}Ne at Deutsches GeoForschungsZentrum (GFZ) in Potsdam (Niedermann et al., 1997). Stable Al was measured using an ICP-OES at the Hebrew University.

Results

In the upper part of the Sedom Formation, ^{10}Be concentrations for SDM 3,4,5 are low and range between 1.1±0.2x10^4 and 1.7±0.5x10^4 atoms g^{-1} quartz (Table 1). ^{26}Al/^{27}Al ratios for these 3 samples are effectively indistinguishable from the ^{26}Al/^{27}Al ratio measured in the blank. Thus, their ^{26}Al/^{10}Be ratios are below current AMS detection limits indicating the extreme antiquity of these sediments. Sample SDM-2 yielded a ^{26}Al/^{27}Al ratio marginally above background, albeit with a large uncertainty. This ratio corresponds to a ^{26}Al concentration of 0.5±0.5x10^4 atoms g^{-1} quartz. Unfortunately, the ^{10}Be/^{9}Be ratio could not be measured for this sample due to a laboratory problem.

^{10}Be concentrations in the Amiaz-1 borehole samples range between 1.0±0.1x10^4 and 1.5±0.2x10^4 atoms g^{-1} quartz. ^{26}Al concentrations are also very low, although in contrast to results for SDM samples, provide measurable ^{26}Al distinguishable from background, and range between 2.0±0.7x10^4 and 2.8±0.7x10^4 atoms g^{-1} quartz (Table 1). Most of the uncertainty is attributed to ^{26}Al/^{27}Al analytical uncertainties that reach 30%. ^{26}Al/^{10}Be ratios range between 1.44±0.45 and 2.09±0.80.

Cosmogenic ^{21}Ne concentrations in two of the Amiaz-1 borehole samples (AMZ-1, AMZ-3) are 6.7±0.7x10^6 atoms g^{-1} quartz and $5.3^{+1.5}_{-1.2}$x10^6 atoms g^{-1} quartz (Table 1). The uncertainties in ^{21}Ne concentrations are large (between 10% and 28%) and are due to large amounts of trapped atmosphere-like Ne (high ^{20}Ne concentrations), and subsequently to rather small excesses in ^{21}Ne/^{20}Ne resulting from cosmic ray production. In the Ne three-isotope diagram of the AMZ samples (Fig. 8a), the isotope ratios for extractions up to 800°C follow a line parallel to the expected spallation line (i.e., the mixing line of atmospheric and cosmogenic Ne; Niedermann et al., 1993) through the data point representing the crushing extraction of AMZ-1, except for the 400°C step of AMZ1 which contributes only ~2% to the total ^{21}Ne excess up to 800°C for this sample. These data are thus consistent with a two-component mixture of fractionated atmospheric and cosmogenic Ne. The 1200°C ratios, however, plot above that mixing line. Because no cosmogenic Ne is released from quartz above 800°C (Niedermann, 2002), these data indicate a contribution of nucleogenic ^{21}Ne and ^{22}Ne from (α,n) reactions on ^{18}O and ^{19}F, respectively. In absolute terms, the 1200°C steps released $3.3\pm0.7\times10^{6}$ and $1.9\pm0.8\times10^{6}$ atoms g^{-1} of excess ^{21}Ne for AMZ-1 and 3, respectively, which is another 50% and 35% of the excess ^{21}Ne released up to the 800°C step. Some contribution of nucleogenic Ne in the lower temperature steps can therefore not be excluded, and the cosmogenic ^{21}Ne concentrations given above must be considered as maximum values.

Higher ^{10}Be concentrations occur in the Cave of the Letters samples. They range between 12.0±0.4x10^{4} and 57.5±1.6x10^{4} atoms g^{-1} quartz. ^{26}Al concentrations range between 49.5±7.2x10^{4} and 69.4±4.2x10^{4} atoms g^{-1} quartz (Table 1). ^{26}Al/^{10}Be ratios range between 1.11±0.10 and 4.32±0.28. These ratios correspond to simple burial ages that range between 0.9±0.1 Ma (COL2) and 3.4±0.2 Ma (COL1) (Fig. 7). Age calculations assume negligible post burial production due to the massive shielding of 70 m of dense dolomite over the cave. Cosmogenic ^{21}Ne concentrations in two of the COL samples (COL-1, COL-2) are 4.3±1.2x10^{6} atoms g^{-1} quartz and 4.05±0.88x10^{6} atoms g^{-1} quartz (Table 1). In this case, the 400-800°C data are consistent with a two-component mixture of unfractionated atmospheric and cosmogenic Ne (Fig. 8b), while the 1200°C data again indicate some contribution of nucleogenic Ne, which is however smaller than for the AMZ samples.

The ^{10}Be concentration in the Masada cave sample (MZ2) is 18.1±0.5x10^{4} atoms g^{-1} quartz, its ^{26}Al concentration is 19.7±7.5x10^{4} atoms g^{-1} quartz (Table 1) and the ^{26}Al/^{10}Be ratio is 1.09±0.42. This ratio corresponds to a simple burial age of 3.6±0.4 Ma (Fig. 7). This age calculation assumes negligible post burial production even though the present geometry of the site suggests only 12-20 m of rock shielding.

Discussion

The age of the Amora and Sedom Formations

TCN results and their corresponding burial ages of the Amora Formation and the top of the

Sedom Formation are in agreement with their stratigraphic position. AMZ samples provide an age range for the base of the Amora Formation between $2.7^{+0.7}_{-0.6}$ Ma (AMZ-1) and $3.3^{+0.9}_{-0.8}$ Ma (AMZ-3) (Fig. 7). Age calculations safely assume negligible post burial production due to the high sedimentation regime and the extraction of the samples directly from a deep borehole, >1000 m below the surface.

^{21}Ne-^{10}Be and ^{21}Ne-^{26}Al ratios of the AMZ samples yield apparent burial ages of ~8.5 Ma and ~6 Ma, respectively. These ages are significantly older than their ^{10}Be-^{26}Al counterpart burial ages. Some contribution of nucleogenic Ne in the lower temperature steps cannot be excluded, and the cosmogenic ^{21}Ne concentrations given above must be considered as maximum values. However, being a stable nuclide, ^{21}Ne can be retained in the quartz grains from previous cycles of exposure. Since Amora Formation sediments include recycled sand from the Miocene Hazeva Formation which by itself consists of recycled Nubian Lower Cretaceous and Lower Paleozoic sands (Sa'ar, 1985), the excess ^{21}Ne in samples AMZ is not surprising.

Dealing with Miocene sediments, which are at the very limit of the cosmogenic burial dating range, places a challenge in determining the ^{26}Al cosmogenic isotope concentrations by AMS. The antiquity of such sediments prevents precise and unambiguous measurements of the ^{26}Al concentrations in the SDM samples. The absence of ^{26}Al in all four SDM samples suggests three rather surprising conclusions when one considers that currently they are exposed surface samples: 1) total burial of the Sedom Formation sediments has been sufficiently long to allow the decay of essentially all the ^{26}Al that was in the quartz at the time of deposition. Assuming a reasonable initial ^{26}Al concentration of ~10^6 atoms g^{-1} (as suggested by sample MK22W; Fruchter et al., 2011) and an AMS minimum detection limit of ~10^4 atoms g^{-1} (Table 1; sample SDM-2), at least 6-7 ^{26}Al half lives have elapsed since sediment burial, which is equivalent to 4.2 – 4.9 Ma, 2) the reduction in shielding as the salt diapir was uplifted and exhumed was rapid, and 3) any recent production of ^{26}Al has been negligible. With a site production rate of ~18 atoms g^{-1} yr^{-1}, accumulation of ^{26}Al would reach the detection limit of ~10^4 atoms g^{-1} (Table 1 sample SDM-2) within 500-1000 yr, assuming instantaneous exposure. Since erosion and surface change on Mt. Sedom are extremely rapid, and noticeable changes, such as gully incision to a depth of several meters, occur in a life time, a recent exposure of ancient deposits for only a few centuries may not be all that surprising. Hence, we consider that recent accumulation of post-burial produced ^{26}Al that would exceed the AMS detection limit to be unlikely.

If the calculation above for ^{26}Al yields a burial age of 4.2 – 4.9 Ma (6-7 half lives), then for the same sand grain and same initial ^{26}Al/^{10}Be input at t=0 we should get the same burial age estimate from the ^{10}Be concentration. Indeed, the initial ^{10}Be concentration would have been 1.5x10^{5} ^{10}Be atoms g^{-1}. This concentration stems from the initial ^{26}Al concentration (as shown above) divided by 6.75 (which is the production rate ratio). From Table 1 we can see that the mean ^{10}Be concentration for SDM samples is 1.3x10^{4} atoms g^{-1}, indicating that ~ 3-4 half-lives (equal to ~4-6 Ma) must have elapsed since burial.

In addition to constraining the minimum age of the SDM samples by the absence of measurable ^{26}Al, we suggest two approaches to better approximate the limits for the Sedom Formation burial ages. First, assuming that all SDM samples were deposited within a relatively short time, such that within the resolution of burial dating they are of similar age, we can combine the ^{26}Al concentration of sample SDM-2 together with the range in ^{10}Be concentrations measured in samples SDM-3, SDM-4, and SDM-5 to estimate representative ^{26}Al/^{10}Be ratios for the SDM samples in order to calculate minimum burial ages. These calculations yielded ^{26}Al/^{10}Be ratios in the range of 0.35-0.52 (see Table 1) which correspond to burial ages in the range of $5.3^{+inf}_{-1.8}$ Ma and $6.2^{+inf}_{-2.1}$ Ma for the top of the Sedom Formation (Fig. 7).

Another independent estimate of the age of the Sedom Formation uses a previously published measurement of the ^{10}Be concentration from presently exposed Hazeva Formation sand (Fruchter et al., 2011). We consider this result to be a reasonable estimate of the initial pre-burial concentration (N_0). Using this value we can calculate the time required to reach the measured ^{10}Be concentrations due to decay. A provenance study of DSF sediments (Sa'ar, 1985) suggests that sands imbedded in the Sedom Formation consist of continental sediments that were transported by an extensive drainage system that flowed from the Trans-Jordanian plateau across the Dead Sea transform to the Mediterranean Sea. Such Miocene sands that accumulated in the DSF and in the Negev Desert belong to the Hazeva Formation (Calvo, 2000). Age estimates for the base of the Hazeva Formation range between 25 Ma and 20 Ma (Steinitz et al., 1978; Calvo, 2002). The age of the top of the Hazeva Formation is older than 8-6 Ma

(Steinitz et al., 2000; Steinitz and Bartov, 1991). Based on mineralogical assemblages, Agnon (1983a,b) estimated that the Sedom Formation was deposited synchronously with the later part of the Hazeva Formation, thus enabling the inclusion of Hazeva Formation sand in the Sedom Formation. If we assume that the concentration of ^{10}Be in these sediments was mostly controlled by the rate at which the Miocene sands were exhumed and transported into the Sedom Lagoon and that such exhumation has been operating continuously, ^{10}Be concentrations in the present outcrops of the Miocene sands should be representative of the sands that were deposited in the Sedom Lagoon. Today, Hazeva Formation sediments are preserved mainly in local structural lows such as synclines and grabens located along the western margin of the DSF. One such location is the Yamin Plane, ~30 km SW of the study site (Fig. 3), a syncline overlain by Hazeva Formation sediments (Hirsch, 1995) and presently drained to the southern end of the Dead Sea. A sand sample (MK22W) collected from a small streambed draining the Yamin Plane was analyzed for ^{26}Al ($95.6\pm9.9\times10^4$ atoms g^{-1} quartz) and ^{10}Be ($16.8\pm0.2\times10^4$ atoms g^{-1} quartz) by Fruchter et al. (2011).

The results of these analyses show that this sample is positioned at the beginning point of a decay line passing through the SDM samples (Fig. 7). If the sample from the Yamin Plane is in fact an appropriate analog for N_0, then the age of the SDM samples can be based solely on the ^{10}Be measurements. This procedure yields an average ^{10}Be burial age of 5.0±0.5 Ma for the top of Sedom Formation. This age approximation agrees with the other age estimation presented above and supports a late Miocene age for the upper part of the Sedom Formation. Since an additional 250 m of Sedom Formation sediments overlie our SDM samples, the actual termination of sediment deposition by the Sedom Lagoon is somewhat younger than the age attributed here. It is interesting to note that Steinitz and Bartov (1991) provided similar age constraints for the Sedom Formation based on a broad examination of the paleogeographical evolution of the DSF by means of radiometric dating of plateau pre-rift basalts and basalts which flowed through incised canyons towards the Dead Sea.

The rise of the Sedom diapir has been examined in numerous multi-disciplinary studies and is reviewed by Weinberger et al. (2006). They conclude that Mt. Sedom breached the surface about 14 ka and very rapid erosion of the soft sediment followed the rise of the mountain. The absence of ^{26}Al and the low levels of ^{10}Be in all the SDM samples forces us to assume that our sampling locations must have been shielded by at least tens of meters of sediment until very recently. Nevertheless, it is instructive to consider the possible effect of post burial production of ^{26}Al on the SDM samples as its absence constrains possible scenarios of diapir emergence. In the context of post-burial production, the exposure history is simplified and divided into two stages: 1) rise of the diapir to the surface through the basin sediments. During this stage, the overburden is well in excess of hundreds to thousands of meters. The contribution of post-burial production of cosmogenic nuclides during the first stage of the diapir uplift through the basin sediments (until 14 ka) is found to be insignificant at a total of ~200 ^{26}Al atoms g^{-1} quartz, considering a rising rate of 5 mm yr^{-1} and a minimum of 20 m of final overburden, and 2) breaching of the surface and the formation of Mt. Sedom. During this stage TCN production can occur. The transition between the two stages took place after the retreat of Lake Lisan at ~14 ka as both alluvial and lake sediments are found on top of Mt. Sedom, disconnected from their surroundings (Fig. 4; Weinberger et al., 2006). The overburden above the SDM samples at the time of the diapir emergence is considered to be at least 50 m: 20 m of current stream incision into the Sedom Formation and ~30 m of overlying Lake Lisan sediments (Weinberger et al., 2007; Fig. 4).

Post-burial production during the second stage could have a noticeable effect on burial ages, depending on the exposure history (Fig. 9). Although erosion of this overburden began immediately after the retreat of Lake Lisan at 14 ka, major stream incision started later as a result of relief development and rapid dissolution of halite within the Sedom Formation. ^{14}C dating of cave passages at different depths places the beginning of incision at ~3.3 ka for the north-eastern boundary of Mt. Sedom (Frumkin, 1996). If erosion of the overburden and late incision (i.e. since 3.3 ka) are assumed as suggested by dated cave passages (Frumkin, 1996), then post-burial production of ^{26}Al may amount to no more than 2000 atoms g^{-1} quartz (if initial overburden after 14 ka was 40 m and final overburden was 1 m; Fig. 9), and no more than 3000 atoms g^{-1} quartz (if initial overburden after 14 ka was 20 m and final overburden was only 0.5 m; Fig. 9). In both these cases the TCN ages presented above may be underestimated by only 0.7-1.3 million yr. If, however, erosion of the overburden and incision started immediately after emergence of the diapir (~14 ka), then post burial production of ^{26}Al may amount to as much as 10,000 atoms g^{-1} quartz (Fig. 9) and the TCN ages presented above may be extremely underestimated. This scenario is not supported by the results of Frumkin (1996), by field evidence that indicates very rapid erosion and incision of the mountain, and by the absence of measurable ^{26}Al.

It should be noted here that we concentrated our discussion concerning post-burial production on ^{26}Al because it is produced much faster than ^{10}Be. Total post burial production of ^{10}Be would range between 300 and 450 atoms g^{-1} quartz, if incision started at 3.3 ka. This amount is within the measuring error of ^{10}Be and would not contribute to any change in the calculated ^{26}Al/^{10}Be ratio. Overall, our results suggest that the age of the top of the Sedom Formation ranges between 5.0±0.5 Ma and $6.2^{+\mathrm{inf}}_{-2.1}$Ma, depending on the different assumptions made in the burial age calculations. These ages lie at the upper limit of the age range of the cosmogenic burial dating method. The absolute age of the Miocene-Pliocene boundary is somewhat debated and ranges between 4.6 and 5.3 Ma (e.g. Hilgen and Langeries, 1993). Our age for the Sedom Formation is taken from 250 meters below the top of the formation and ranges between $6.2^{+inf}_{-2.1}$ and 5.0±0.5 Ma. Therefore, the age of the very top of the Sedom Formation maybe very early Pliocene. Of course, this constrains a Miocene age for most of the Sedom formation sediments.

Cave ages

Sediment burial ages have been used to estimate the time when active drainage systems operated at the level of cave openings (e.g. Granger et al. 1997, 2001; Stock et al., 2004; Haeuselmann et al., 2007; Wagner et al., 2010). In this study, we date the oldest sediments relating to active drainage or shoreline activity are preserved within caves close to the top of the escarpment (Frumkin, 2001; Lisker et al., 2010). Sediment burial ages in the Masada cave (MZ2) would be indicative of the time the surface of the Dead Sea basin was at the level of the cave. Similarly, sediment burial ages in the Cave of the Letters would indicate the time the floor of Wadi Hever canyon was at the level of the cave while incising into the desert plateau in response to subsidence of the Dead Sea basin. Therefore, as both caves are relatively close to the top of the escarpment, burial ages of sediment trapped in them would represent the initial stages of rapid subsidence of the Dead Sea basin and formation of significant relief in the region.

Apart from sample COL3, collected from the front face of the sedimentary cave fill, which was exposed by canyon side-cliff retreat, all other Cave of the Letters samples were collected from deep within the cave (>10 m from the entrance) and are well shielded. Nevertheless, Cave of the Letters samples do not converge to a common burial age. We suspect that biogenic activity, namely the presence of wasp nests in the cave, is responsible for this age scatter. Wasps collect wet silt and fine sand from potholes in the canyons and use it when building their nests in the cave. Wasps have been nesting in the soft sediments of the Cave of the Letters since the passages in the cave were excavated ~2000 yr ago by humans. Therefore, the samples we collected, although not showing evidence of present wasp activity, may have been contaminated with silt and fine sand brought in by wasps during the past 2000 yr. Therefore, the resultant $^{26}Al/^{10}Be$ ratio and calculated burial age depend on the ratio of sand deposited in the cave when the cave was at the level of the active drainage system and wasp-delivered sediment. Any addition of silt which postdates cave abandonment and thus characterized by higher $^{26}Al/^{10}Be$ ratios, to the sample would result in an underestimation of the burial age. The observation of possible mixing of ancient cave sediment with modern sediment is supported by the location of all the COL samples on the Al-Be burial plot (Fig. 7). All COL samples fall on a mixing curve between modern sediment and undisturbed cave sediment. We therefore, consider the oldest age as representing the minimum burial age of the sediment in the cave. This age of 3.4±0.2 Ma is given by sample COL1, which was collected 21 m from the entrance of the cave. Since the cave opening is located ~70 m below the upper desert surface, incision must have started some time prior to this age.

The burial age given by sample COL1 enables to calculate an average bedrock incision rate (~0.07 mm yr^{-1}) of Wadi Hever since the deposition of the Cave of the Letters sediments. This rate is slightly higher than those calculated in the southern Sierra Nevada during times of tectonic quiescence but an order of magnitude lower during major uplift, 3-1.5 Ma (Stock et al., 2005). Similarly, incision rate in Wadi Hever is similar to that calculated in the eastern Alps for the past 2.5 Ma but an order of magnitude slower than the eastern Alps in the Pliocene (Wagner et al., 2010). The more active Swiss (western) Alps have been incised an order to two orders of magnitude faster (Haeuselmann et al., 2007). Overall, the incision rate calculated for the DSF canyon is similar to those calculated in other regions of moderate tectonic activity. In contrast, it is somewhat faster than those calculated in regions of tectonic quiescence, such as in the Appalachian Mountains (Granger et al., 1997, 2001). It must be kept in mind, however, that in Wadi Hever, and in all other canyons that drain into the Dead Sea, incision slowed down dramatically during periods of lake high stand, such as the late Pleistocene Lake Lisan high stand between 20-30 ka (Bartov et al., 2002; Lisker et al., 2009). This implies, of course, that incision must have been more rapid during other times.

It is interesting to consider the burial age calculated for sample COL3 that was collected at the front of the cave, where the sedimentary section is exposed by the horizontal retreat of the canyon cliff. The age given by this sample (3.0±0.1 Ma) is only 0.4 Ma younger than the oldest age given by sample COL1. This decrease in the calculated burial age is most likely caused by the production of ^{26}Al and ^{10}Be in the sediments as they were exhumed at the front of the cave by the retreating canyon wall. If actually caused by recent exposure, the increase in the ^{26}Al/^{10}Be ratio from 1.11 (COL1) to 1.45 (COL3), would take only ~15 ka if the face was exposed instantaneously (using a site ^{10}Be production rate of ~2.5 atoms g^{-1} yr^{-1} and a ^{26}Al production rate of ~16.9 atoms g^{-1} yr^{-1}). However, this is a theoretical end-member case. The retreat rate of the major knick point of Wadi Hever was estimated to range between 800 and 1600 mm ka^{-1} (Haviv et al., 2006) and cliff retreat rates that range between 100 and 850 mm ka^{-1} have been published for various arid regions in the world (e.g. Schumm and Chorley, 1966; Yair and Gerson, 1974; Mayer, 1979; Cole and Mayer, 1982; Matmon et al., 2005). Applying cliff retreat rates in the range of 100 to 800 mm ka^{-1}, implies that the time required to shift the ^{26}Al/^{10}Be ratio from 1.11 to 1.45 would be longer but that the sediments presently exposed at the front of the cave were shielded until recently.

^{21}Ne-^{10}Be and ^{21}Ne-^{26}Al ratios of sample COL2 yield apparent burial ages of 2.4 Ma and 1.9 Ma, respectively. These ages are older than the ^{10}Be-^{26}Al burial age of this sample (0.9 Ma). It is reasonable that some of the quartz grains transported into the Cave of the Letters by Wadi Hever originated from Miocene Hazeva sand outcrops that existed on the Judea Desert Plateau during the Pliocene. Therefore, as with the AMZ samples, the excess in the cosmogenic ^{21}Ne concentrations can be explained by its accumulation during previous cycles of exposure and its retention in the quartz crystals.

In contrast to sample COL2, ^{21}Ne-^{10}Be and ^{21}Ne-^{26}Al ratios of sample COL1 yield apparent burial ages of 0.5 Ma and 2.3 Ma, respectively. These ages are younger than the ^{10}Be-^{26}Al burial age of this sample (3.4 Ma). It is difficult to explain such a result as typically ^{21}Ne based ages generally equal or exceed those determined using $^{26}Al/^{10}Be$ ratios. Other than instrumental or analytical errors, field related complications could result in diffusive loss of ^{21}Ne, most likely through heating. During Roman times, 2000 yr ago, the Cave of the Letters was occupied for over a century (this is the cave in which many of the Dead Sea ancient documents were found and the reason for its name). We conjecture that frequent use of small camp fires would be sufficient to heat the sand in the immediate surrounding of the hearth to several hundred degrees causing diffusive loss of Ne from quartz grains but not affecting the ^{10}Be and ^{26}Al concentrations. Niedermann (2002) showed that a high percentage (up to 70%) of cosmogenic ^{21}Ne is loosed from quartz grains at temperatures <600°C. This would result in underestimated ^{21}Ne-^{10}Be and ^{21}Ne-^{26}Al burial ages. Such a process has been previously suggested to explain the loss of other noble gases from rock samples (Gillespie et al., 1985). Although speculative, we offer this scenario as a possible explanation for the relatively low Ne concentration.

The $^{26}Al/^{10}Be$ ratio in the Masada cave (sample MZ2) is 1.09±0.42. This ratio corresponds to a simple burial age of 3.6±0.4 Ma. At this site we did not observe any wasp activity. However, shielding of the sediment is not as thick as in the Cave of the Letters. MZ2 burial age is identical within error to the age of sample COL1 (3.4±0.2 Ma) and suggests that post-burial production is not significant. This points to the possibility that shielding must have been greater than observed toady during most of the time that the sediment of sample MZ2 was buried. Based on the burial ages of the cave sediments, initial incision and relief formation along the Dead Sea escarpment was well expressed by ~3.5 Ma.

Implications for the morphotectonic evolution of the Dead Sea basin and its western margin

Stein et al. (2000) observed discordant dolomitic bodies along the western margin of the Dead Sea basin that attest to intense dolomitization, which occurred within the Upper Cretaceous limestone by interaction with highly evaporated sea water that filled the basin. Ryb et al. (2009a,b) studied iron mineralization of veins included in these dolomitic bodies and emphasized the involvement of evaporated sea water in the process. Using U-Pb, Ryb et al.

(2009a) dated the mineralized veins to 11.8±2.0 Ma. The geomorphic implication of these observations and results is that the structure, and more importantly the topography of the western margin of the Dead Sea fault enabled, at that time, the penetration of Mediterranean water into the transform valley and the formation of saline marine lagoons. Although this process has been proposed and described earlier (Katz and Starinsky, 2009), the work of Ryb et al. (2009a) was the first to provide robust age constraints. Passage between the evolving transform valley and the Mediterranean was possible as long as low topography persisted along the western margin of the Dead Sea fault. The new cosmogenic nuclide age determinations provided here for the top of the Sedom Formation, between 5.0±0.5 Ma and $6.2^{+inf}_{-2.1}$ Ma, and for the base of the overlying Amora Formation, $3.3^{+0.9}_{-0.8}$ Ma, constrain the time that this passage ceased and terminal lakes commenced. Based on these ages, the transition from water bodies connected to the Mediterranean to those not connected may have occurred roughly between 5 and 3.5 Ma. This time range is essential in any further research of the Quaternary topographic evolution and the contemporary drainage pattern development of the western margin of the DSF.

Why did such a transition occur at that time? A change of only a few degrees in the direction of motion of the Arabian plate relative to the African plate would introduce an extension component to the Dead Sea fault and trigger significant subsidence (to form a rift) and significant uplift of the margins. Such a change in the direction of motion has been previously proposed to explain observations of major importance. To the south, Bosworth et al., (2005) estimate that the rate of extension increases at ~5 Ma which is followed by the first appearance of MORB in the Red Sea. To the north, Westaway, (2004) observes that the East Anatolian fault (EAF) was initiated at ~4 Ma following the change in stress field. Both these observations point to an increase in the E-W vector of the motion of the Arabian plate (Fig. 1). Such a change would introduce noticeable extension along the Dead Sea fault. We suggest that the timing of increased rift subsidence and major relief expression along the Dead Sea segment of the Arabian-African plate boundary, based on our new cosmogenic burial ages, is commensurate with the tectonic modifications observed in the Red Sea to the south and Anatolian Fault to the north.

Changes in the direction of plate motion over time scales of 10^6 yr are not a unique event (e.g.

Sharp and Clague, 2006). Nor is the reorganization of plate boundary directions. The direction of the Arabia-African plate boundary has changed over time, as did the direction of relative motion between the two plates. For example, at 14–12 Ma a major structural event occurred along the northern part of the Arabia-African plate boundary. Tectonic activity decreased dramatically along the Gulf of Suez, which is the northern and direct extension of the Red Sea, the Red Sea motion switched from rift-normal movement to highly oblique extension and strike slip motion commenced along the DSF (Bosworth et al., 2005). Steckler and ten Brink (1986) suggested that the cause for this switch in plate boundary configuration was the inability of the Red Sea rift to propagate northward through the stronger lithosphere of the Mediterranean continental margin. Later research (e.g. Bosworth and McClay, 2001) established that, although the greater strength of the Mediterranean continental margin lithosphere did play a role in determining the Red Sea plate boundary geometry, it was not in as complete a fashion as previously thought.

A change of smaller magnitude occurred along the Arabia-African plate boundary in the Pliocene. Garfunkel (1981) analyzed the kinematics of the DSF motion and concluded that Miocene motion along the plate boundary had to be of a more N-S direction than that of the Pliocene to prevent inconsistent overlap of lithospheric portions of the Arabian and African plates. Joffe and Garfunkel (1987) showed that the slip rates for the Miocene (~6.5 km Ma^{-1}) were slower than those calculated for the Pliocene-Pleistocene (~9 km Ma^{-1}). These rates also agree with initial observations by Quennell (1951, 1958). Late Quaternary slip rates as well as present ones, based on GPS measurements, are slower and are on average 5 km Ma^{-1} (LeBeon et al., 2010, 2012; Daëron et al., 2004, 2007; McClusky et al., 2003).

The association between rift subsidence and margin uplift has been described for several rifts (Rosendahl, 1987; Wdowinski and Zilberman, 1996, 1997; ten-Brink et al., 1990). Uplifted rift shoulders are recognized in rifts of various ages (e.g. Bloom, 1998; Hutchinson et al., 1992; Bohannon et al., 1989). Furthermore, the memory of uplifted rift margins from a time of significant tectonic activity still persists along most continental passive margins (van der Beek and Braun, 1999; Gilchrist and Summerfield, 1994; Beaumont et al., 2000). We argue that the transition from a subdued topography of the Sedom Lagoon during the late Miocene to the more contemporary disconnected water bodies such as documented over the more recent

Quaternary is the consequence of the initiation of significant subsidence along the DSF accompanied by significant margin uplift (Wdowinski and Zilberman, 1996, 1997) about 5-3 Ma. The subsequent construction of a continuous water divide west of the rift then allowed major fluvial incision along the evolving escarpment. These processes dominated the slip along the DSF long enough to modify the drainage system pattern and significantly affect sediment transport and deposition capabilities throughout the Quaternary. Consequently, in contrast to the tectonic evolution of the Dead Sea fault that started at about 18 – 14 Ma but did not affect topography in a significant way for at least 10 Ma, the style of deformation since 5 Ma and into the Quaternary, which included rifting, also controlled the evolution of the current drainage systems and topographical framework of the water bodies in the DSF valley.

The oldest burial age of alluvial sediments derived from the Cave of the Letters (3.4±0.2 Ma) and the burial age derived from the sediment in the Masada cave (3.6±0.4 Ma) indicate that incision had commenced earlier than ~3.5 Ma and that significant relief had also been present. The cave sediment burial ages obtained in this study are similar to other age constraints of initial canyon incision related to Dead Sea subsidence. On the eastern side of the Dead Sea, in the Zarka Ma'in canyon region (Fig. 3), a flood basalt located on the plateau and dated to ~6 Ma (Steinitz and Bartov, 1991) indicates that incision initiated after it flowed. On the other hand, about 100 m below the Jordanian desert plateau and 200 m above the Zarka Ma'in canyon floor, a younger basalt that flowed towards the rift through the entrenched canyon was dated using K-Ar to 3.4 Ma (Steinitz and Bartov, 1991). This age is identical to the burial ages given by the cave sediments on the western DSF margin. Furthermore, the basalt is positioned in the canyon below the desert plateau at a similar elevation as the Cave of the Letters, suggesting that along both margins flanking the Dead Sea basin, incision began at roughly similar times and that initial canyons were already formed. The beginning of relief formation along the DSF western margin is implied by other observations, such as the water-table fall in the northern Negev dated by U-Pb of the earliest vadose cave deposits to ~3.1 Ma (Vaks et al., 2013) and by exhumation, exposure to air oxygen, and combustion of bituminous rocks that occurred between 3.8 and 2.6 Ma along the western margin of the Dead Sea (Gur et al., 1995).

Similar age constraints are obtained from the northern part of the Dead Sea fault. In the northern Jordan Valley, the Yarmuch canyon incises between the Jordanian Plateau and the

Golan Heights into Pliocene flood basalts (the Cover Basalt Formation) which flowed prior to incision and are dated to ~4.5 Ma (Mor and Steinitz, 1985; Shaliv, 1991). Thus, incision of this major canyon began after 4.5 Ma as a response to major DSF subsidence. Davis et al. (2011) dated the first fresh water body in the Jordan Valley (the Erk El Ahmar Lake) to ~4.5 Ma. The sediments of this lake overlie the Cover Basalt Formation (Rotstein et al., 1992; Inbar et al., 2010), and although of the same age, their stratigraphic order indicates that the lake sediments were deposited immediately after the basalt covered the region. The presence of a fresh water body indicates that disconnection from the Mediterranean Sea and formation of non-terminal fresh water bodies (similar to present-day Sea of Galilee) had occurred by 4.5 Ma. Our results from the region of the Dead Sea and the results presented above from the northern Jordan Valley, ~200 km north, suggest a similar time, 5-4 Ma, for the disconnection of the rift valley from Mediterranean Sea. This similarity suggests that significant subsidence accompanied by margin uplift and the establishment of the western water divide occurred simultaneously. These processes, therefore, set the scene for the Quaternary morphologic development and sedimentologic regime of the entire DSF western margin.

Conclusions

Direct radiometric dating of deeply buried Dead Sea intra-rift and rift shoulder sediments was possible for the first time using TCN measurements. Complexities due to post-burial production were avoided by sampling from a deep borehole (bottom of Amora Formation), from sediments which were rapidly uplifted from within the deep basin by a rising diapir (Sedom Formation), and sediments that were buried in caves. These approaches enabled the burial dating of late Miocene and Pliocene sediments – pushing the limit of the cosmogenic burial dating method. The absence of ^{26}Al in the top of the Sedom Formation sediments indicates both the antiquity of the sediments and the very rapid exposure by the rising diapir. Using different constraining methods and assumptions these sediments are dated to 6-5 Ma. The oldest Amora Formation sample, collected from ~50 m above the base of the formation, yielded a TCN burial age of $3.3^{+0.9}_{-0.8}$ Ma. ^{21}Ne ages of the Amora Formation and of cave sediments do not conform to the ^{26}Al-^{10}Be burial ages due to ^{21}Ne retention in the quartz grains from previous erosional episodes.

Burial ages of cave sediments range between 3.6 and 3.4 Ma and suggest initial incision of canyons flowing into the Dead Sea shortly before this time. These ages agree well with other indications of topographic relief and incision from other locations along the fault. We show that the major difference between the Sedom Lagoon and the later water bodies is the consequence of the initiation of DSF significant subsidence accompanied by significant uplift of the its margins, and the establishment of a continuous water divide west of the DSF. The change in the style of faulting along the DSF coincides with the first MORB's in the Red Sea and the initiation of the East Anatolian fault. All of these processes resulted from a change in the direction of motion of the Arabian plate relative to the African plate. Along the Dead Sea rift, this change was followed by a dramatic reorganization of relief and drainage patterns in the region.

Acknowledgments

This study was supported by the ISF-Bikura grant 362/06 and Hebrew University Ring internal grant. We thank Roi Porat and Uri Davidovich who noted to us the potential significance of the Masada cave sediments to the rift margin evolution.

References

Agnon, A., 1983a. An attempted revision of the Neogene stratigraphy in the Dead Sea Valley. Israel Geological Society Annual Meeting, Nazareth, p. 63.

Agnon, A., 1983b. The development of depositional basins in the southern part of western Dead Sea escarpment. M.Sc. thesis, Hebrew University of Jerusalem, 61 p.

Agnon, A., 1993. The fault escarpment south west of the Dead Sea: From stratigraphy to morphotectonic history. Israel Geological Society Annual Meetings, Field Trips Guidebook, Arad, Israel, pp. 81-97.

Avni, Y., Bartov, Y., Garfunkel, Z., Ginat, H., 2000. Evolution of the Paran drainage basin and its relations to the Plio-Pleistocene history of the Arava Rift western margin, Israel. Israel Journal of Earth Sciences 49, 215-238.

Balco, G., Shuster, D.L., 2009. Production rate of cosmogenic ^{21}Ne in quartz estimated from ^{10}Be, ^{26}Al, and ^{21}Ne concentrations in slowly eroding Antarctic bedrock surfaces, Earth and Planetary Science Letters 281, 48-58.

Balco, G., Stone, J.O., Lifton, N.A., Dunai, T.J., 2008. A complete and easily accessible means of calculating surface exposure ages or erosion rates from ^{10}Be and ^{26}Al measurements. Quaternary Geochronology 3, 174-195.

Bartov, Y., Steinitz, G., Eyal, M., Eyal, Y., 1980, Sinistral movement along the Gulf of Aqaba - its age and relation to the opening of the Red Sea. Nature 285 (5762), 220-222.

Bartov, Y., Stein, M., Enzel, Y., Agnon, A., Reches, Z., 2002. Lake Levels and Sequence Stratigraphy of Lake Lisan, the Late Pleistocene Precursor of the Dead Sea. Quaternary Research 57 (1), 9–21.

Beaumont, C., Kooi, H., Willett, S., 2000. Coupled tectonic-surface process models with applications to rifted margins and collisional orogens. *in* Summerfield, M.A., ed., Geomorphology and global tectonics: Chichester, John Wiley, 29–55.

Begin, Z. B., Ehrlich, A., Nathan, Y., 1974. Lake Lisan; the Pleistocene precursor of the Dead Sea, Bulletin - Geological Survey of Israel 63, 38.

Belmaker, B., Lazar, B., Beer, J., Christl, M., Tepelyakov, N., Stein, M., 2013. ^{10}Be dating of Neogene halite. Geochimica et Cosmochimica Acta 122, 418–429.

Bierman, P.R. Caffee, M.W., 2001. Slow rates of rock surface erosion and sediment production across the Namib Desert and escarpment, Southern Africa. American Journal of Science 301 (4-5), 326-358.

Bloom, A.L., 1998. Geomorphology (third edition): Upper Saddle River, New Jersey, Prentice Hall, 482 p.

Bohannon, R.G., Naeser, C.W., Schmidt, D.L., Zimmermann, R.A., 1989. The timing of uplift, volcanism and rifting peripheral to the Red Sea: A case for passive rifting?. Journal of Geophysical Research 94, 1683–1701.

Bosworth, W., Huchon, P., McClay, K., 2005. The Red Sea and Gulf of Aden Basins. Journal of African Earth Sciences 43, 334–378.

Bosworth, W., McClay, K., 2001. Structural and stratigraphic evolution of the Gulf of Suez rift, Egypt: A synthesis. In: Ziegler, P.A., Cavazza, W., Robertson, A.H.F., Crasquin-Soleau, S., (Eds.), Peri-Tethys Memoir 6: Peri-Tethyan Rift/Wrench Basins and Passive Margins, MeÅLmoires du MuseÅLum National d_Histoire Naturelle de Paris 186, 567–606.

Braucher, R., Merchel, S., Borgomano, J., Bourlès, D.L., 2011. Production of cosmogenic radionuclides at great depth: A multi element approach. Earth and Planetary Science Letters 309, 1-9.

Calvo, R., 2002. Stratigraphy and petrology of the Hazeva Formation in the Arava and Negev: Implications for the development of sedimentary basins and morphotectonics of the Dead Sea Rift valley. Geological Survey of Israel report, GSI/22/02, 264p.

Calvo, R., 2000. Stratigraphy and petrology of the Hazeva Formation in the Arava and the Negev: implications for the development of sedimentary basins and the morphotectonics of the Dead Sea Rift Valley. PhD thesis [in Hebrew], Earth Sciences Department. Hebrew University, Jerusalem.

Calvo, R., Bartov, Y., 2001. Hazeva Group, southern Israel: New observations, and their implications for its stratigraphy, paleogeography, and tectono-sedimentary regime. Israel Journal of Earth Sciences 50, (2-4), 71-99.

Chmeleff, J., von Blanckenburg, F., Kossert, K. Jakob, D., 2010. Determination of the ^{10}Be half-life by multicollector ICP-MS and liquid scintillation counting. Nuclear Instruments & Methods in Physics Research Section B-Beam Interactions with Materials and Atoms 268 (2), 192-199.

Cole, K.L., Mayer, L., 1982. Use of packrat middens to determine rates of cliff retreat in the eastern Grand Canyon, Arizona. Geology 10 (11), 597– 599.

Daëron, M., Klinger, Y., Tapponnier, P., Elias, A., Jacques, E., Sursock, A., 2007. 12,000-year long record of 10 to 13 paleo-earthquakes on the Yammoûneh fault (Levant fault system, Lebanon). Bulletin of the Seismological Society of America 97 (3), 749-771.

Daëron, M., Benedetti, L., Tapponnier, P., Sursock, A., Finkel, R., 2004. Constraints on the post ~25-ka slip rate of the Yammoûneh fault (Lebanon) using in situ cosmogenic ^{36}Cl dating of offset limestone-clast fans. Earth and Planetary Science Letters 227 (1–2), 105–119.

Davis, M.N., Matmon, A., Ron, H., Fink, D., Niedermann, S., 2011. Dating Pliocene lacustrine sediments in the central Jordan Valley, Israel - Implications for cosmogenic burial dating. Earth and Planetary Science Letters 305, 317-327.

Dunai, T.J., 2001. Influence of secular variation of the geomagnetic field on production rates of in situ produced cosmogenic nuclides. Earth and Planetary Science Letters 193, 197-212.

Ebinger, C.J., 1989. Tectonic development of the western branch of the East African rift system. Geological Society of America Bulletin 101, 885–903.

Ebinger, C.J., Rosendahl, B.R., and Reynolds, D., 1987. Tectonic model of the Malawi rift, Africa. Tectonophysics 141, 215– 235.

Fink, D., Smith, A., 2007. An inter-comparison of ^{10}Be and ^{26}Al AMS reference standards and the ^{10}Be half-life. Nuclear Instruments and Methods in Physics Research, Section B (Beam Interactions with Materials and Atoms) 259, 600-609.

Fruchter, N., Matmon, A., Avni, Y., Fink, D., 2011. Sediment source and mixing and the cycle of sediment transport: an example from NE Negev Desert, Israel. Geomorphology 134, (3-4), 363-377.

Frumkin, A., 1996. Determining the exposure age of a karst landscape. Quaternary Research 46, 99-106.

Frumkin, A., 2001. The Cave of the Letters Sediments—Indication of an Early Phase of the Dead Sea Depression?. The Journal of Geology 109 (1), 79-90.

Frumkin, A., 2009. Formation and dating of a salt pillar in Mount Sedom diapir, Israel. Geological Society of America Bulletin 121 (1/2), 286–293.

Garfunkel, Z., 1981. Internal structure of the Dead Sea leaky transform (rift) in relation to plate kinematics. Tectonophysics 80, 81-108.

Garfunkel, Z., Horovitz, A., 1966. The upper tertiary and quaternary morphology of the Negev. Israel Journal of Earth Sciences 15, 101-117.

Gilchrist, A.R., Summerfield, M.A., 1994. Tectonic models of passive margin evolution and their implications for theories of long-term landscape evolution, *in* Kirkby, M.J., ed., Process models and theoretical geomorphology: Chichester, John Wiley and Sons, p. 55–84.

Gillespie, A.R., Budinger Jr., F.E., Abbott, E.A., 1989. Verification of prehistoric campfires by ^{40}Ar/^{39}Ar analysis of fire-baked stones. Journal of Archaeological Science 16 (3), 271–291.

Gosse, J.C. Phillips, F.M., 2001. Terrestrial in situ cosmogenic nuclides: theory and application. Quaternary Science Reviews 20 (14), 1475-1560.

Granger, D.E., 2006. A review of burial dating methods using ^{26}Al and ^{10}Be. Special Paper - Geological Society of America, 415, 1-16.

Granger, D.E., Fabel, D., Palmer, A.N., 2001. Pliocene-Pleistocene incision of the Green River, Kentucky, determined from radioactive decay of cosmogenic ^{26}Al and ^{10}Be in Mammoth Cave sediments. Geological Society of America Bulletin 113, 825-836.

Granger, D.E., Kirchner, J.W. Finkel, R.C., 1997. Quaternary downcutting rate of the New River, Virginia, measured from differential decay of cosmogenic ^{26}Al and ^{10}Be in cave-deposited alluvium. Geology 25 (2), 107-110.

Gur, D., Steinitz, G., Kolodny, Y. Starinsky, A., McWilliams, M., 1995. $^{40}Ar/^{39}Ar$ Dating of Combustion Metamorphism (the "Mottled Zone", Israel). Chemical Geology 122, 171-184.

Guralnik, B., Matmon, A., Avni, Y., Fink, D., 2010. ^{10}Be exposure ages of ancient desert pavements reveal Quaternary evolution of the Dead Sea drainage basin and rift margin tilting. Earth Planetary Science Letters 290, 132-141.

Haeuselmann, P., Granger, D.E., Jeannin, P.Y., Lauritzen, S.E., 2007. Abrupt glacial valley incision at 0.8 Ma dated from cave deposits in Switzerland. Geology 35 (2), 143–146.

Haviv, I., Enzel, Y., Whipple, K. X., Zilberman, E., Stone, J., Matmon, A., Fifield, L. K. 2006. Amplified erosion above waterfalls and oversteepened bedrock Reaches. Journal of Geophysical Research 111, F04004.

Hirsch, F., 1995. 1:50,000 Geological map, Sheet 19-II (Hanakhtesh Haqatan). Geological Survey of Israel.

Horowitz, A., 2001. The Jordan Rift Valley. Taylor & Francis.

Hutchinson, D.R., Golmshtok, A.J., Zoneneshain, L.P., Moore, T.C., Scholz, C.A., Klitgord, K.D., 1992. Depositional and tectonic framework of the rift basins of Lake Baikal from multichannel seismic data. Geology 20, 589–592.

Inbar, N., Shulman, H., Flexer, A., Yellin-Dror, A., 2010. The structure of Kinnarot Basin, Jordan Rift Valley, Israel. The Israel Geological Society, Annual Meeting Abstract Book, p. 77.

Kashai, E.L. Croker, P.F., 1987. Structural geometry and evolution of the Dead Sea-Jordan rift system as deduced from new subsurface data. Tectonophysics 141 (1-3), 33-60.

Katz, A., Starinsky, A., 2009. Geochemical history of the Dead Sea. Aquatic Geochemistry 15, 159-194.

Kaufman, A., 1971. U-series dating of Dead Sea basin carbonates. Geochimica et Cosmochimica Acta 35, 1269–1281.

Ken-Tor, R., Agnon, A., Enzel, Y., Stein, M., Marco, S., Negendank, J.F.W. , 2001a. High-resolution geological record of historic earthquakes in the Dead Sea basin. Journal of Geophysical Research 106 (n B2), 2221-2234.

Ken-Tor, R., Stein, M., Enzel, Y., Agnon, A., Marco, S., Negendank, J.F.W., 2001b. Precision of calibrated radiocarbon ages of historic earthquakes in the Dead Sea Basin. Radiocarbon 43 (n 3), 1371-1382.

Korschinek, G., et al., 2010. A new value for the half-life of ^{10}Be by Heavy-Ion Elastic Recoil Detection and liquid scintillation counting. Nuclear Instruments & Methods in Physics Research Section B-Beam Interactions with Materials and Atoms 268 (2), 187-191.

LeBeon, M., Klinger, Y., Al-Qaryouti, M., Meriaux, A.S., Finkel, R.C., Elias, A., Mayyas, O., Ryerson, F., Tapponnier, P., 2012. Quaternary morphotectonic mapping of the Wadi Araba and implications for the tectonic activity of the southern Dead Sea fault**. Tectonics 31 (5),** DOI: 10.1029/2012TC003112

LeBeon, M., Klinger, Y., Al-Qaryouti, M., Meriaux, A.S., Finkel, R.C., Elias, A., Mayyas, O., Ryerson, F., Tapponnier, P., 2010. Early Holocene and Late Pleistocene slip rates of the southern Dead Sea Fault determined from ^{10}Be cosmogenic dating of offset alluvial deposits. Journal of Geophysical Research: Solid Earth 115, DOI: 10.1029/2009JB007198.

Lisker, S., Vaks, A., Bar-Matthews, M., Porat, R., Frumkin, A., 2009. Stromatolites in caves of the Dead Sea Fault Escarpment: implications to latest Pleistocene lake levels and tectonic subsidence, Quaternary Science Reviews, 28, 1-2, 80-92.

Lisker, S., Porat, R., Frumkin, A., 2010. Late Neogene rift valley fill sediments preserved in caves of the Dead Sea Fault Escarpment (Israel): palaeogeographic and morphotectonic implications. Sedimentology 57, 429–445.

Mack, G.H., Seager, W.R., Leeder, M.R., Perez-Arlucea, M., Salyards, S.L., 2006. Pliocene and Quaternary history of the Rio Grande, the axial river of the southern Rio Grande rift, New Mexico, USA. Earth-Science Reviews 79 (1-2), 141-162.

Marco, S., 1996. Paleomagnetism and Paleoseismology in the Late Pleistocene Dead Sea Graben. Ph.D. Thesis, The Hebrew University of Jerusalem.

Matmon, A., Shaked, Y., Porat, N., Enzel, Y., Finkel R., Lifton, N., Boaretto, E., Agnon, A., 2005. Landscape development in an hyper arid sandstone environment along the margins of the Dead Sea fault: implications from dated rock falls. Earth and Planetary Science Letters 240, 803-817.

Matmon, A., Zilberman, E., Enzel, Y., 2000. Determination of escarpment age using morphologic analysis: An example from the Galilee, northern Israel. Geological Society of America Bulletin 112 (12), 1864-1876.

Matmon, A., Enzel, Y., Zilberman, E., Heimann, A., 1999. Late Pliocene to Pleistocene Reversal of Drainage Systems in Northern Israel: Tectonic Implications. Geomorphology 28, 43-59.

Mayer, L., 1979. Evolution of the Mogollon Rim in central Arizona, Tectonophysics 61, 49– 62.

McClusky, S., Reilinger, R., Mahmoud, S., Ben Sari, D., Tealeb, A., 2003. GPS constraints on Africa (Nubia) and Arabia plate motions. Geophysics Journal International 155, 126–138.

Mor, D., Steinitz, G., 1985. K-Ar ages of the Neogene-Quaternary basalts around the Yarmuk Valley, Annual Meeting - Israel Geological Society, 77-78.

Neev, D., 1960. A pre-Neogene erosion channel in the southern Coastal Plain of Israel. Geological Survey of Israel Bulletin 25, 20.

Neev, D., Emery, K.O., 1967. The Dead Sea, depositional processes and environments of evaporates. Israel Geological survey Bulletin 41, 147 p.

Niedermann, S., 2002. Cosmic-ray-produced noble gases in terrestrial rocks: Dating tools for surface processes. Reviews in Mineralogy and Geochemistry 47, 731-784.

Niedermann, S., Graf, T. Marti, K., 1993. Mass spectrometric identification of cosmic-ray-produced neon in terrestrial rocks with multiple neon components. Earth and Planetary Science Letters 118, 65-73.

Niedermann, S., Bach, W. Erzinger, J., 1997. Noble gas evidence for a lower mantle component in MORBs from the southern East Pacific Rise: decoupling of helium and neon isotope systematics. Geochimica et Cosmochimica Acta 61, 2697-2715.

Nishiizumi, K., 2004. Preparation of ^{26}Al AMS standards. Nuclear Instruments and Methods in Physics Research, Section B (Beam Interactions with Materials and Atoms) 223-224, 388-92.

Ollier, C.D., 1995. Tectonics and landscape evolution in southeast Australia. Geomorphology 12, (1), 37-44.

Pe'eri, S., Zebker, H. A., Ben-Avraham, Z., Frumkin, A., Hall, J. K., 2004. Spatially-resolved uplift rate of the Mount Sedom (Dead Sea) salt diapir from InSAR observations. Israel Journal of Earth Sciences 53 (2), 99-106.

Picard, L., 1943. Structure and evolution of Palestine with comparative notes on neighboring countries. Hebrew University of Jerusalem, Geology Department Bulletin 4, 134 p.

Quennell, A.M., 1951. Geology and mineral resource of (former) Transjordan. Colonial Geology and Mineral Resources 2, 85–115.

Quennell, A. M., 1958. The Structural and Geomorphic Evolution of the Dead Sea Rift. Quaterly Journal of the Geological Society of London 114, 1-24.

Rood, D.H., Hall, S., Guilderson, T.P., Finkel, R.C., Brown, T.A., 2010. Challenges and opportunities in high-precision ^{10}Be measurements at CAMS. Nuclear Instruments and Methods in Physics Research Section B: Beam Interactions with Materials and Atoms 268, 730-732.

Rosendahl, B.R., 1987. Architecture of continental rift with special reference to East Africa. Annual Review of Earth and Planetary Sciences 15, 445–503.

Rotstein, Y., Bartov, Y., Frieslander, U., 1992. Evidence for local shifting of the main fault and changes in the structural setting, Kinarot Basin, Dead Sea transform. Geology 20, 251–254.

Ryb, U., Mattews, A., Erel, Y., Gordon, G., Anbar, A., Avni, Y., 2009a. Iron mineralization along the northern Negev anticlines: sources, timing, and paleogeographical implications. Israel Geological Society, Annual meeting abstracts, p. 112.

Ryb, U., Erel, Y., Mattews, A., Avni, Y., Gordon, G., Anbar, A., 2009b. Large Molybdenium isotope variations trace subsurface fluid migration along the Dead Sea transform. Geology 37 (5), 463-466.

Sa'ar, H., 1985. Origin and sedimentology of the sandstones in graben-fill formations of Dead Sea Rift Valley. M.Sc. Thesis, Hebrew University, 81 pp.

Sharp, W.D., Clague, D.A., 2006. 50-Ma Initiation of Hawaiian-Emperor Bend Records Major Change in Pacific Plate Motion. Science 313, 1281-1284.

Schumm, S.A., Chorley, R.J., 1966. Talus weathering and scarp recession in the Colorado Plateaus. Z. Geomorphol. 10, 11 – 36.

Shaliv, G., 1989. Stages in the tectonic and volcanic history of Neogen continental basins in northern Israel. PhD thesis, Hebrew University, p. 102.

Shaliv, G., 1991. Stages in the tectonic and volcanic history of the Neogene basin in the Lower Galilee and the valleys. Geological Survey of Israel, Report GSI/11/91. 101 pp.

Steckler, M.S., ten Brink, U.S., 1986. Lithospheric strength variations as a control on new plate boundaries; examples from the northern Red Sea region. Earth and Planetary Science Letters 79, 12159–12173.

Stein, M., Agnon, A., 2007. So, what is the age of the Sedom Lagoon? Annual Meeting - Israel Geological Society, Newe Zohar, p. 119.

Stein, M., Agnon, A., Starinsky, A., Raab, M., Katz, A., Zak, I., 1994. What is the "age" of the Sedom Formation? Annual Meeting - Israel Geological Society 1994, p. 108.

Stein, M., Starinsky, A., Agnon, A., Katz, A., Raab, M., Spiro, B., Zak, I., 2000. The impact of brine-rock interaction during marine evaporite formation on the isotopic Sr record in the oceans: Evidence from Mt. Sedom, Israel. Geochimica et Cosmochimica Acta 64, 2039-2053.

Steinitz, G., Bartov, Y., Hunziker, J.C., 1978. K-Ar age determinations of some Miocene-Pliocene basalts in Israel and their significance to the tectonics of the rift valley. Geological Magazine 115, 329-340.

Steinitz, G., Bartov, Y., 1991. The Miocene-Pliocene history of the Dead Sea segment of the rift in light of K-Ar ages of basalts. Israel Journal of Earth-Sciences, 40 (1-4), 199-208.

Steinitz, G., Calvo, R., Bartov, Y., 2000. New ^{40}Ar-^{39}Ar age for the Ein Yahav dike and its implications on the age of the Hazeva Formation. Geological Survey of Israel, Current Research 12, 206-208.

Stock, G.M., Anderson, R.S., Finkel, R.C., 2004. Pace of landscape evolution in the Sierra Nevada, California, revealed by cosmogenic dating of cave sediments. Geology 32, 193–196.

Stock, G.M., Anderson, R.S., Finkel, R.C., 2004. Rates of erosion and topographic evolution of the Sierra Nevada, California, inferred from cosmogenic ^{26}Al and ^{10}Be concentrations. Earth Surface Processes and Landforms 30, 985–1006.

Summerfield, M. A., 1991a. Sub-aerial denudation of passive margins; regional elevation versus local relief models. Earth and Planetary Science Letters 102 (3-4), 460-469.

Summerfield, M. A., 1991b. Global geomorphology; an introduction to the study of landforms, 537 p. Longman Science and Technology. John Wiley & Sons, Essex, United Kingdom, New York, NY, United States

ten-Brink, U.S., Schoenberg, N., Kovach, R.L., Ben-Avraham, Z., 1990. Uplift and possible Moho offset across the Dead Sea transform. In: Kovach R.L. and Ben-Avraham, Z. eds., Geologic and Tectonic Processes of the Dead Sea Transform Zone. Tectonophysics 180, 71-85.

Torfstein, A., 2008. Brine freshwater interplay and effects on the evolution of saline lakes: the Dead Sea rift terminal lakes, Ph.D. thesis, The Hebrew University of Jerusalem.

Torfstein, A., Haase-Schramm, A., Waldmann, N., Kolodny, Y., Stein, M., 2009. U-series and oxygen isotope chronology of the mid-Pleistocene Lake Amora (Dead Sea basin). Geochimica et Cosmochimica Acta 73, 2603–2630.

Vaks, A., Woodhead, J., Bar-Matthews, M., Ayalon, A., Cliff, R., Zilberman, T., Matthews, A., Frumkin, A., 2013. Pliocene-Pleistocene climate of the northern margin of Saharan-Arabian Desert recorded in speleothems from the Negev Desert, Israel. Earth and Planetary Science Letters 368, 88-100.

van der Beek, P., Braun, J., 1999. Controls on post mid-Cretaceous landscape evolution in the southeastern highlands of Australia: Insights from numerical surface process models. Journal of Geophysical Research 104, 4945–4966.

Wagner, T., Fabel, D., Fiebig, M., Haeuselmann, P., Sahy, D., Xu, S., Stuwe, K., 2010. Young uplift in the non-glaciated parts of the Eastern Alps. Earth and Planetary Science Letters 295 (1-2), 159-169.

Wdowinski, S., Zilberman, E., 1996. Kinematic modeling of large scale structural asymmetry across the Dead Sea Transform. Tectonophysics 266, 187–201.

Wdowinski, S., Zilberman, E., 1997. Systematic analyses of the large-scale topography and structure across the Dead Sea Rift. Tectonics 16, 409– 424.

Weinberger, R., Bar-Matthews, M., Levi, T., Begin, Z.B., 2007. Late-Pleistocene rise of the Sedom diapir on the backdrop of water-level fluctuations of Lake Lisan, Dead Sea basin. Quaternary International 175, 53-61.

Weinberger, R., Begin, Z.B., Waldmann, N., Gardosh, M., Baer, G., Frumkin, A., Wdowinski, S., 2006. Quaternary rise of the Sedom Diapir, Dead Sea basin. Special Paper - Geological Society of America 401, 33-51.

Westaway, R., 2004. Kinematic consistency between the Dead Sea Fault Zone and the Neogene and Quaternary left-lateral faulting in SE Turkey. Tectonophysics 391, 203– 237.

Yair, A., Gerson, R., 1974. Mode and rate of escarpment retreat in an extremely arid environment. Z. Geomorphol., Suppl. 21, 202– 215.

Zak, I., 1967. The Geology of Mt. Sedom. PhD Thesis, Hebrew University, Jerusalem.

Zelilidis, A., 2000. Drainage evolution in a rifted basin, Corinth graben, Greece. Geomorphology 35 (1-2), 69-85.

Zilberman, E., Baer, G., Avni, Y., Feigin, D., 1996. Pliocene fluvial systems and tectonics in the central Negev, southern Israel. Israel Journal of Earth Sciences 45 (3), 113-126.

Zilberman, E., 1993. The Mahmal Graben and Nahal Hawwa; an introduction to the paleogeography of the central Negev in the Miocene. Israel Journal of Earth-Sciences 42 (3-4), 197-209.

Figure captions

Figure 1: Satellite image of the Middle East marking the location of the major plate boundaries around the Arabian Plate. The Dead Sea fault (DSF) transforms motion between the spreading zones in the south (marked with dash-point lines) and the convergence in the north (marked with dashed lines). EAF - East Anatolian fault. NAF - North Anatolian fault. Location of 5 Ma MORB in Red Sea is marked with red circle. Location of pole of rotation between the African and Arabian plates (Westaway. 2004) is marked with star.

Figure 2: Composite stratigraphic column of the Dead Sea Group (Zak, 1967). Sampled sections are marked with red open boxes. Notice that most of Sedom Formation, particularly within its uppermost ~250 m, is composed of halite and not amenable for cosmogenic $^{26}Al/^{10}Be$ burial dating except for the Benot Lot memeber section (at ~1500 m). The Amora Formation is mostly detrital.

Figure 3: A) Shaded relief map with locations of study sites (marked with yellow dots) within the Dead Sea rift valley (marked with a blue line). The speculated extent of the Sedom Lagoon is marked with a light gray polygon. Sites marked with red dots indicate

locations mentioned in discussion (EEA is Erk el Ahmer) but not sampled for TCN in this study. B) Close-up shaded relief image with TCN sample locations (yellow dots): (1) SDM samples at Mt. Sedom. (2) AMZ samples from the Amora Formation collected from the Amiaz-1 borehole. (3) Surface sediment sample derived from the Yamin Plane (sample MK22W from the Hazeva Formation; Fruchter et al., 2011).

Figure 4: A) Schematic geological cross section through the Mt. Sedom diapir (Frumkin, 2009) showing the location of the SDM samples within the diapir and the Amiaz-1 borehole from which AMZ samples were collected. Subvertical lines are bedding planes. Black dotted filled polygon capping Mt. Sedom represents late Pleistocene Lake Lisan sediments that were uplifted by the rising diapir. These sediments can also be seen as horizontal beds in the upper right side of the photo in (C). B) Photograph showing the landscape presented in (A) with the Pleistocene Lake Lisan sediments in the foreground. C) Photograph of sampling site of the SDM samples on the eastern edge of Mt. Sedom (persons in photo for scale). Sediment beds of the Sedom formation are overturned (~28° dip to the west) due to the uplift of the salt. Late Pleistocene Lake Lisan sediments appearing at the top of the photo are horizontal.

Figure 5: The Cave of the Letters. The main cave entrance is marked with a white polygon which includes the 13.5 m thick sediment fill truncated by the cliff. Sample COL 3 was collected from this truncated wall. The entrance to the passage in the soft sediment that was excavated ~2000 yr ago by humans can be seen at the top of the white polygon. Left inset: Samples COL 1 and COL 2 were collected inside this passage 15-21 m from its entrance. Samples COL 5 and COL 7 were collected from the middle passage, with its entrance indicated by the arrow. Both these samples were collected >10 m from the entrance of the middle passage. The upper desert plateau is ~70 m above the cave opening. The right inset shows a close-up of sedimentary cross bedding in the soft sediment and some wasp drillings in the upper part of the photo.

Figure 6: The Masada Cave. (A) Photo, from south to north, of the Dead Sea escarpment showing Masada, as part of the escapement, in the foreground. The general location of Masada Cave shown in (B) is marked with open box. (B) A series of natural caves exposed below the ruins of the Masada archeological site. The sampled cave is marked

with a black arrow. (C) A measured cross section of the cave indicates the location of sample MZ2 (full dot). Well-cemented sediment is exposed at three locations: a conglomerate on the upper desert surface above the cave, slope debris at the entrance of the cave, and fine shoreline sediments deep at the back of the cave where it is cemented to the bedrock wall. The shoreline sandy sediments are bedded and include mostly chert fragments.

Figure 7: Burial ages for Amora Formation (AMZ) samples, Sedom Formation (SDM) samples, and cave samples (COL, MZ) plotted on a ^{10}Be vs. $^{26}Al/^{10}Be$ exposure-burial diagram. Also shown is a modern analog for possible pre-burial concentrations of Sedom samples (sample MK22W in Fruchter et al., 2011). Notice that all COL samples fall on a mixing curve (designated by an empty elongated rectangle) of ancient buried sediment and modern exposed sediment.

Figure 8: Ne stepwise heating extraction results: a - for samples AMZ-1 and AMZ-3. b - for samples COL-1 and COL-2. 2σ uncertainties are shown in both panels. Extraction temperatures: white- 400°C, gray- 600°C, red- 800°C, black- 1200°C, green- crusher extraction. Crusher extraction measurement is available only for sample AMZ-1 and COL-2. mfl – mass fractionation line.

Figure 9: Simulations of post-burial production of ^{26}Al in SDM samples as a function of the initial overburden (20-40 m) at the time the diapir breached the surface and the time when this overburden started eroding (14-3 ka). Lines in A and B are equal-concentration lines. (A) Simulations considering sample collection after removing 100 cm of surface sediment cover. If erosion of the overburden (~40 m) and late incision, since 3.3 ka, are assumed as suggested by dated cave passages (Frumkin, 1996), then post-burial production of ^{26}Al may amount to no more than 2000 atoms g^{-1} quartz. (B) Simulations considering samples collection after removing 50 cm of cover. If erosion of the overburden (~20 m) and late incision, since 3.3 ka, are assumed as suggested by dated cave passages (Frumkin, 1996), then post-burial production of ^{26}Al may amount to no more than 3000 atoms g^{-1} quartz. (C) In both end member cases described in (A) and (B), the TCN ages presented above may be underestimated by only 0.7-1.3 Ma. The initial burial age that corresponds to zero post-burial production (i.e. 6.2 Ma) is derived from

the ratio of $^{26}Al/^{10}Be$ based on $0.5x10^4$ atoms of ^{26}Al g^{-1} quartz measured in sample SDM-2 and $1.56x10^4$ atoms of ^{10}Be g^{-1} quartz measured in sample SDM-3. X axis indicates ^{26}Al atoms produced only during exhumation in the last 14 ka that are subtracted from the initial ^{26}Al concentration ($0.5x10^4$ atoms g^{-1} quartz) to estimate the true burial age. As the fraction of post-burial ^{26}Al increases it lowers the true $^{26}Al/^{10}Be$ ratio and hence correlates to a longer burial age. Parameters used in the calculation: altitude: -300 m, overburden density: 2 g cm^{-3}, average dipole moment: $8x10^{22}$ Am^2, scaling: Dunai (2001), muon production: Braucher et al. (2011), spallation production: Balco et al. (2008).

Table 1: Cosmogenic nuclide data

Sample name	Quartz (g)	Be carrier (mg)	Al carrier (mg)	Al (ICP-OES) (10^{18} atoms g^{-1})	$^{26}Al/^{27}Al$ ($\times 10^{-15}$)	^{26}Al ($\times 10^{4}$ atoms g^{-1})	Be spike ($\times 10^{17}$ atoms g^{-1})	$^{10}Be/^{9}Be$ ($\times 10^{-15}$)	^{10}Be ($\times 10^{4}$ atoms g^{-1})	$^{26}Al/^{10}Be$	$^{26}Al/^{10}Be$ Corrected[d]
SDM-2[a]	40.037	0.286	0	2.79±0.11	1.9±1.9[c]	0.5±0.5	4.77	N/A	N/A	N/A	N/A
SDM-3[b]	35.002	0.300	0.49	2.99±0.12	**< 9**	< 2.7	5.73	27.2±5.8	1.56±0.34	< 1.7	0.35
SDM-4[b]	35.007	0.299	0.49	3.20±0.13	**< 21**	< 6.7	5.71	29.1±9.0	1.66±0.52	< 4.1	0.33
SDM-5[b]	35.010	0.298	0.49	2.89±0.12	**< 12**	< 3.5	5.69	18.4±3.8	1.05±0.22	< 3.3	0.52
AMZ-1[a]	35.009	0.307	0	3.15±0.13	8.8±2.2	2.77±0.71	5.86	24.6±1.8	1.44±0.12	1.92±0.51	
AMZ-2[a]	35.482	0.303	0	3.05±0.12	6.6±2.4	2.02±0.74	5.71	16.9±1.6	0.96±0.10	2.09±0.80	
AMZ-3[a]	35.003	0.306	0	3.23±0.13	7.7±2.2	2.13±0.62	5.84	25.4±2.9	1.48±0.18	1.44±0.45	
COL1[a]	35.061	0.294	0.491	5.74±0.23	111±8	63.5±5.2	5.60	988±19	57.5±1.6	1.11±0.10	
COL2[a]	35.074	0.295	0.496	4.44±0.18	175±6	59.6±3.2	5.62	237±7	13.8±0.5	4.32±0.28	
COL3[a]	26.971	0.300	0.293	7.07±0.28	147±7	69.4±4.2	7.43	620±15	47.8±1.5	1.45±0.10	
COL5[a]	35.024	0.222	0.160	5.38±0.22	92±13	49.5±7.2	4.24	402±9	12.0±0.4	4.11±0.61	
COL7[a]	35.005	0.235	0.134	7.34±0.29	89±9	65.2±7.4	4.48	858±20	27.2±0.8	2.40±0.28	
MZ2[a]	34.171	0.199	0.141	1.02±0.04	19.4±7.4	19.7±7.5	3.90	657±14	18.1±0.5	1.09±0.42	

Sample name	^{21}Ne (10^{6} atoms·g^{-1})
AMZ-1	6.7±0.7
AMZ-3	5.3 +1.5/-1.2
COL-1	4.3±0.6
COL-2	4.05±0.44

SDM samples are from the Sedom Formation. AMZ samples are from the base of the Amora Formation collected from the Amiaz-1 borehole. COL samples are from the Cave of the Letters. Sample MZ2 is from the Masada cave.

AMZ-1 collected from 1180-1212 m borehole depth, AMZ-2 collected from 1585-1640 m borehole depth, AMZ-3 collected from 1686-1723 m borehole depth.

$^{26}Al/^{27}Al$ ratios in bold indicate no ^{26}Al counts were measured. The ratio presented here was calculated assuming one count.

[a] Measured at LLNL. $^{10}Be/^{9}Be$ were normalized to 07KNSTD3110 = 2.85×10^{-12}. $^{26}Al/^{27}Al$ were normalized to KNSTD 10650 = 1.065×10^{-11}.

$^{10}Be/^{9}Be$ procedural blank was 21.2±1.1x10^{-15}. Standard reference materials at both ANSTO and LLNL are self-consistent.
[b] Measured at ANSTO. $^{10}Be/^{9}Be$ were normalized to NIST SRM-4325 = 2.790×10^{-11}. $^{26}Al/^{27}Al$ were normalized to Vogt SRM Z93-0221 = 1.680×10^{-11}.
$^{10}Be/^{9}Be$ average of procedural blanks was 20.1±2.0x10^{-15}.
[c] Sample SDM-2 had a relatively high $^{26}Al/^{27}Al$ background ratio (2.4x10^{-15}).
[d]Ratio calculated with ^{26}Al concentration of sample SDM-2 and ^{10}Be concentrations of the respective samples.

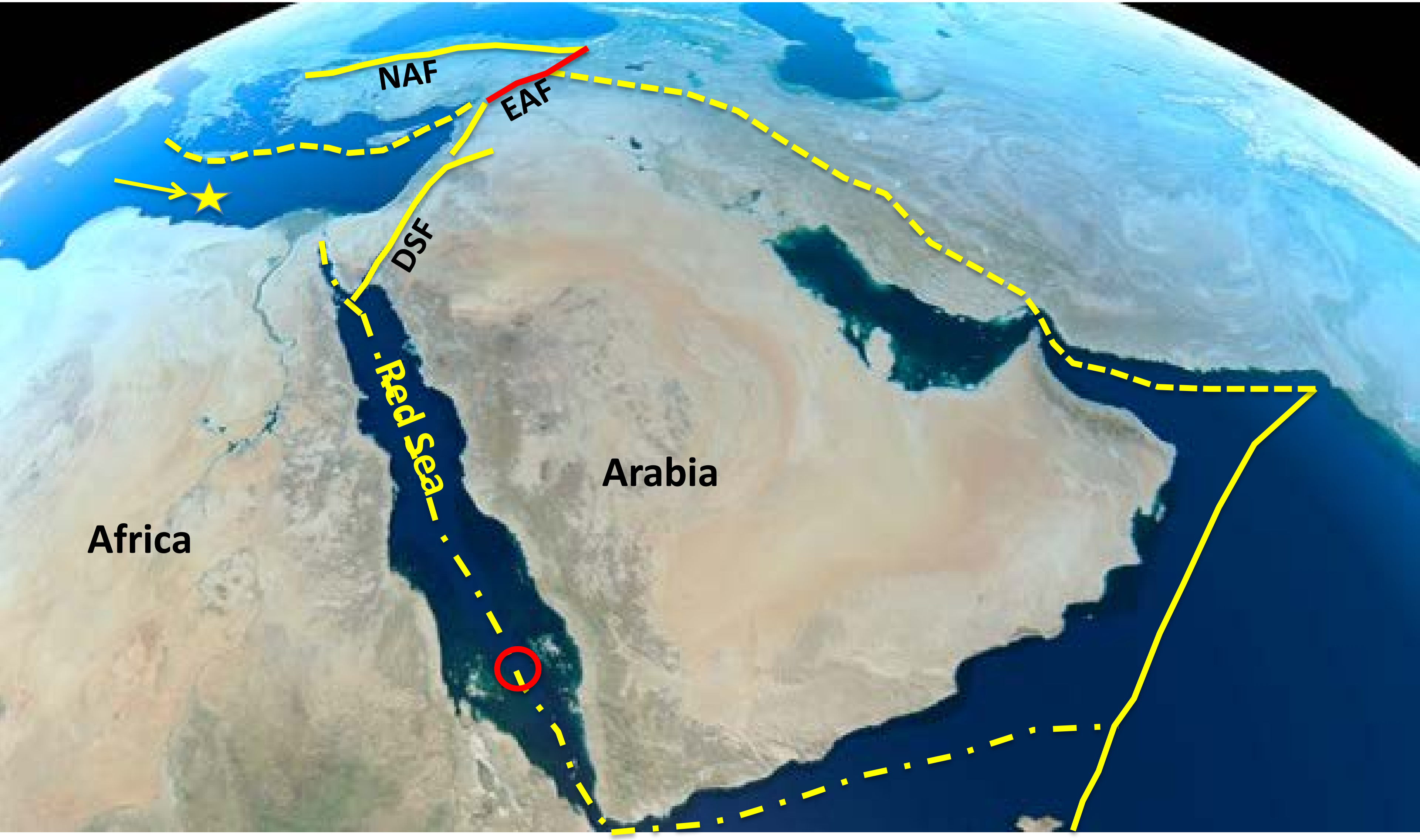

Figure 1

Figure 2

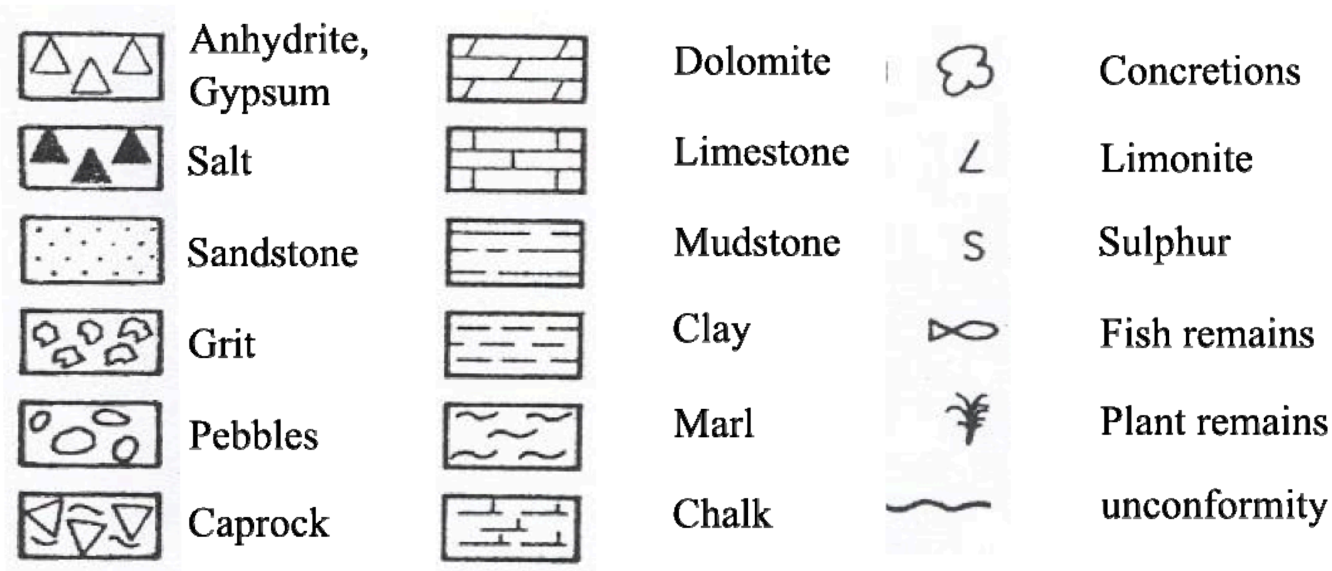

Anhydrite, Gypsum
Salt
Sandstone
Grit
Pebbles
Caprock
Dolomite
Limestone
Mudstone
Clay
Marl
Chalk
Concretions
Limonite
S
Sulphur
Fish remains
Plant remains
unconformity

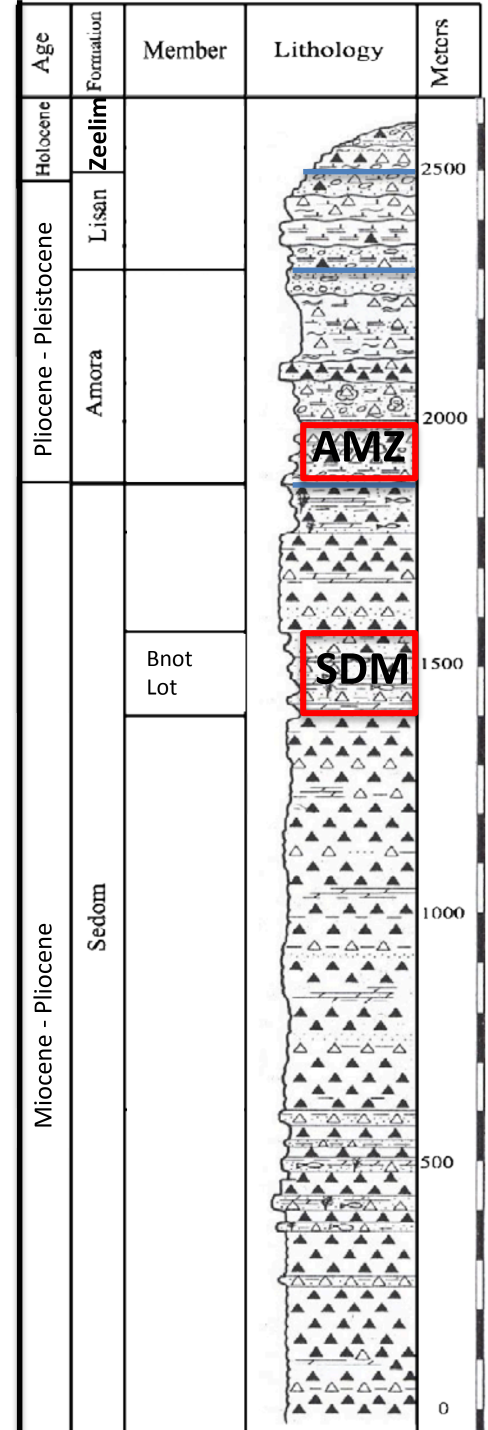

Age
Formation
Member
Lithology
Meters
Holocene
Zeelim
Pliocene - Pleistocene
Lisan
Amora
Miocene - Pliocene
Sedom
Bnot Lot
AMZ
SDM
2500
2000
1500
1000
500
0

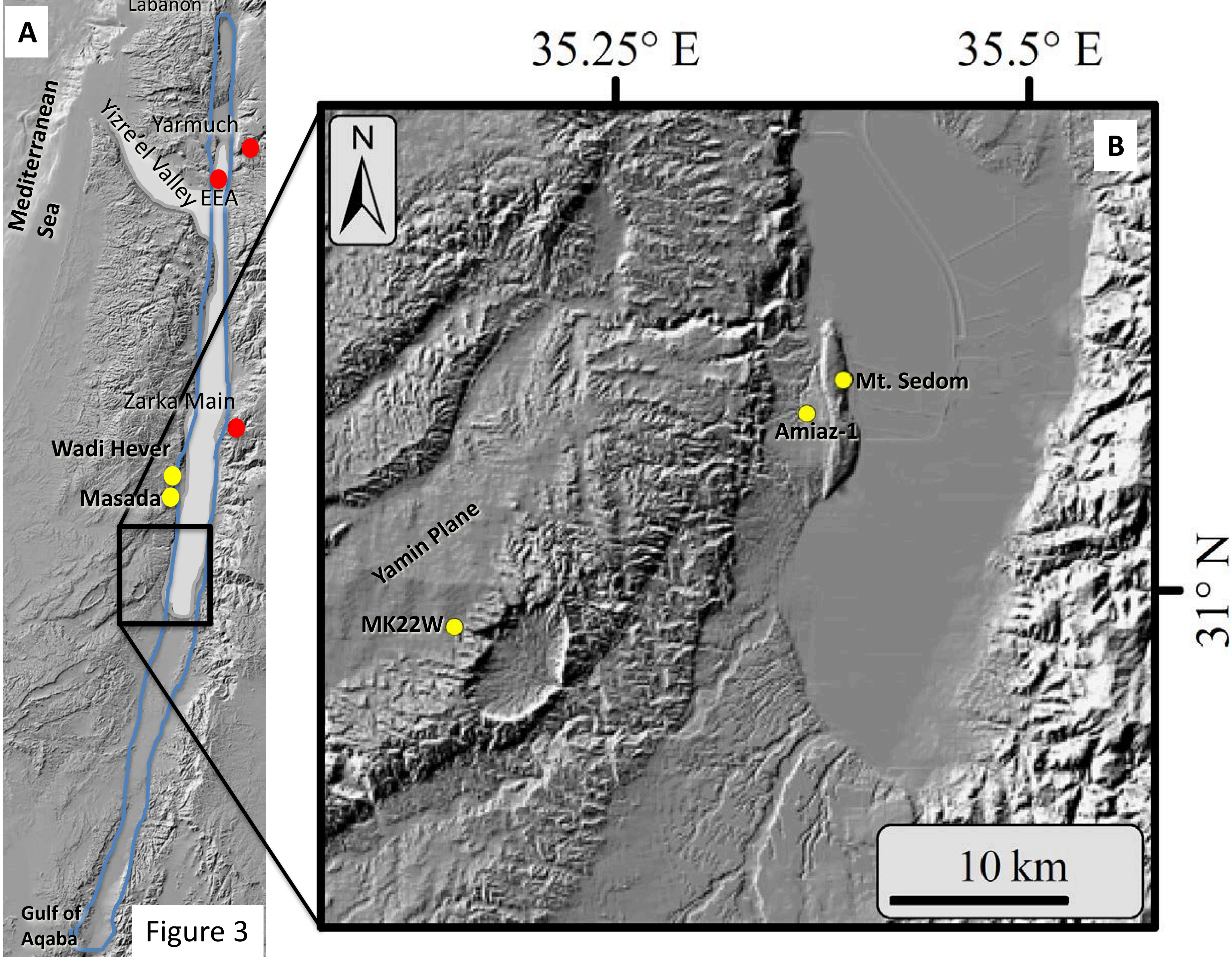
A
Labanon
Mediterranean Sea
Yizre'el Valley
Yarmuch
EEA
Zarka Main
Wadi Hever
Masada
Gulf of Aqaba
35.25° E
35.5° E
31° N
N
B
Mt. Sedom
Amiaz-1
Yamin Plane
MK22W
10 km

Figure 3

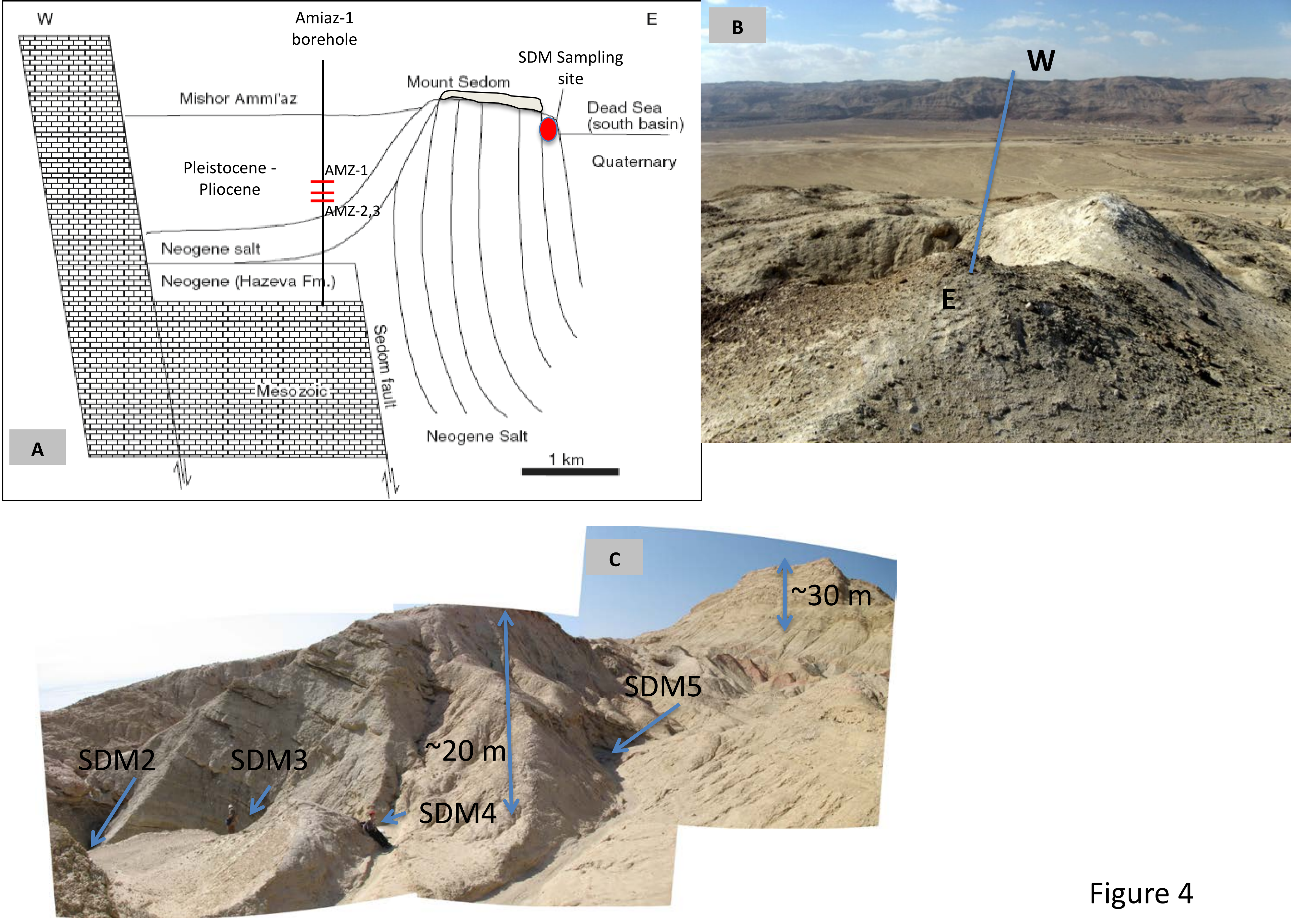
A
W
E
Amiaz-1 borehole
SDM Sampling site
Mount Sedom
Mishor Ammi'az
Dead Sea (south basin)
Quaternary
Pleistocene - Pliocene
AMZ-1
AMZ-2,3
Neogene salt
Neogene (Hazeva Fm.)
Mesozoic
Sedom fault
Neogene Salt
1 km
B
W
E
C
~30 m
~20 m
SDM2
SDM3
SDM4
SDM5

Figure 4

Figure 5

Figure 6

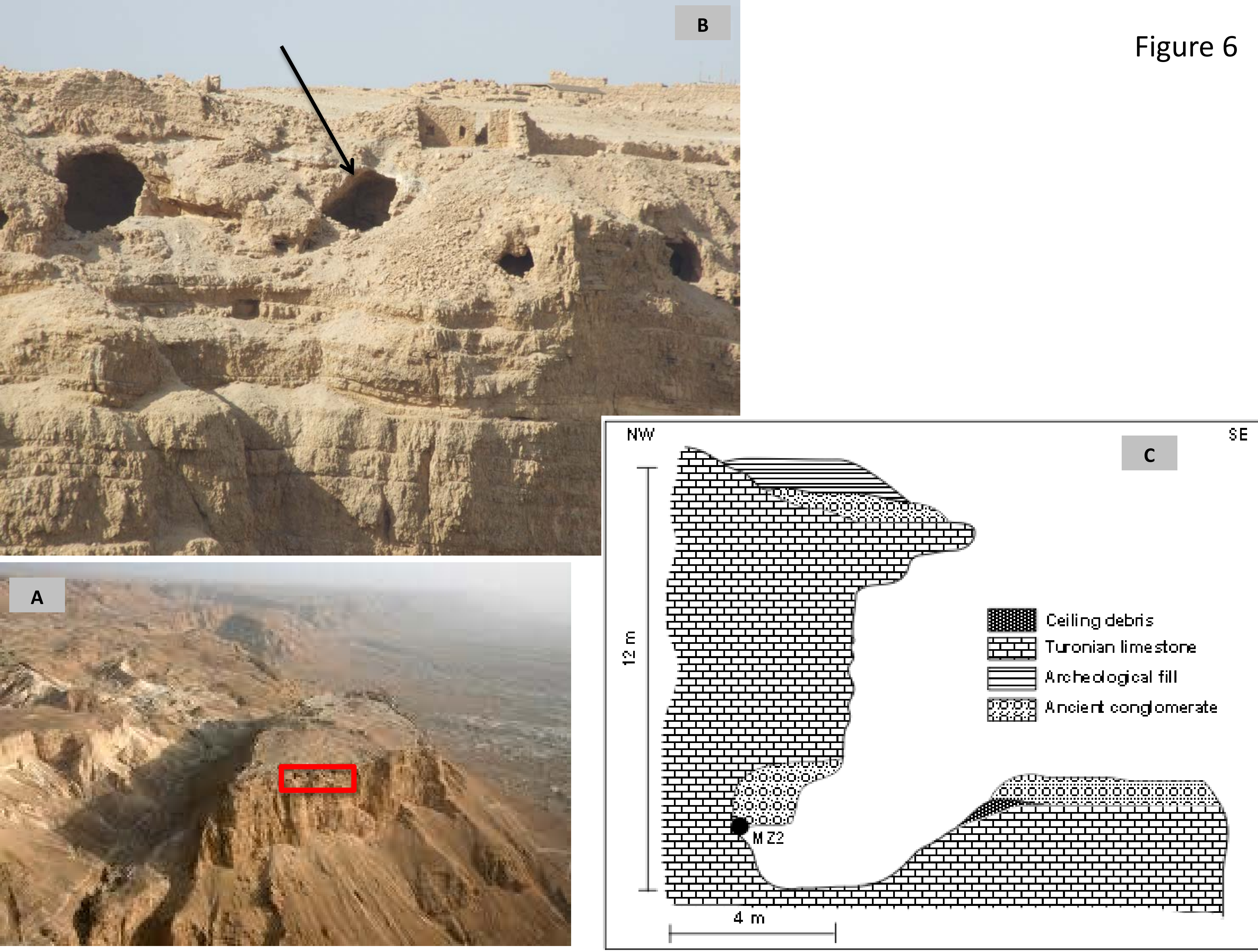

B
A
NW
SE
C
12 m
4 m
MZ2
Ceiling debris
Turonian limestone
Archeological fill
Ancient conglomerate

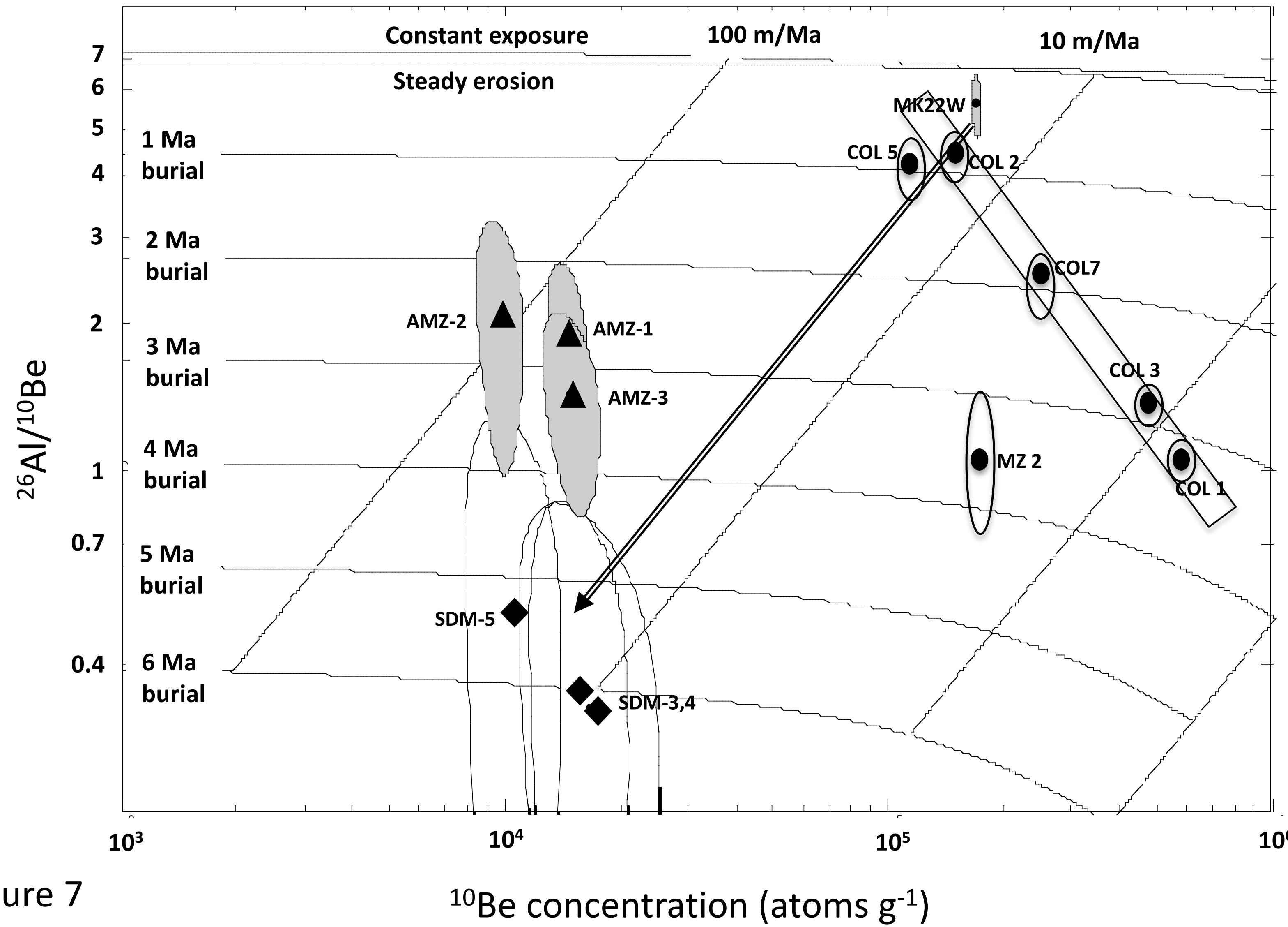

Constant exposure
100 m/Ma
10 m/Ma
Steady erosion
1 Ma burial
2 Ma burial
3 Ma burial
4 Ma burial
5 Ma burial
6 Ma burial
MK22W
COL 5
COL 2
COL7
COL 3
COL 1
MZ 2
AMZ-2
AMZ-1
AMZ-3
SDM-5
SDM-3,4
7
6
5
4
3
2
1
0.7
0.4
10^3
10^4
10^5
10^6
$^{26}Al/^{10}Be$
^{10}Be concentration (atoms g^{-1})

Figure 7

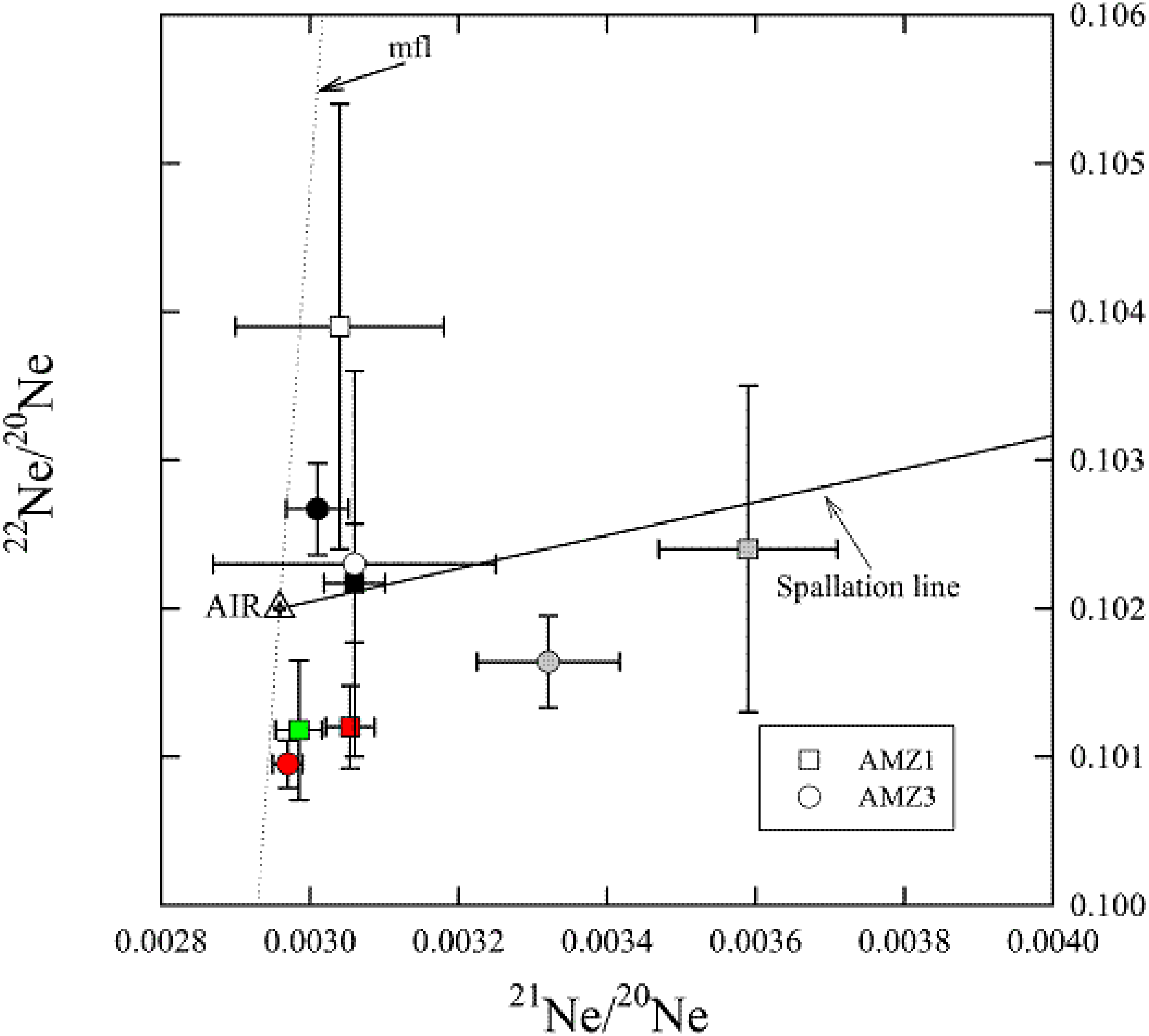
mfl
AIR
Spallation line
AMZ1
AMZ3
0.106
0.105
0.104
0.103
0.102
0.101
0.100
0.0028
0.0030
0.0032
0.0034
0.0036
0.0038
0.0040
$^{22}Ne/^{20}Ne$
$^{21}Ne/^{20}Ne$

Figure 8a

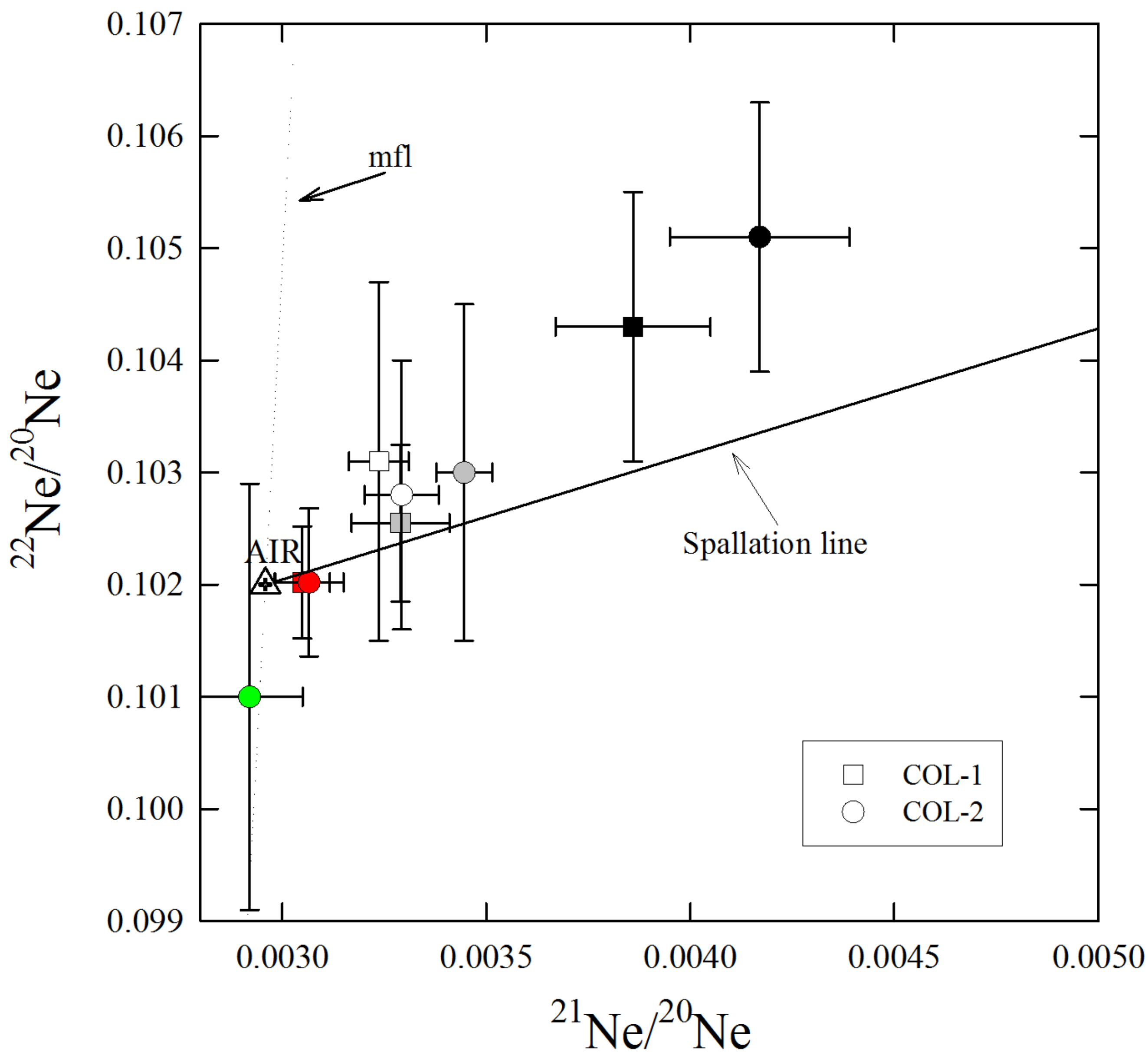
0.107
0.106
0.105
0.104
0.103
0.102
0.101
0.100
0.099
mfl
AIR
Spallation line
COL-1
COL-2
0.0030
0.0035
0.0040
0.0045
0.0050
$^{22}Ne/^{20}Ne$
$^{21}Ne/^{20}Ne$

Figure 8b

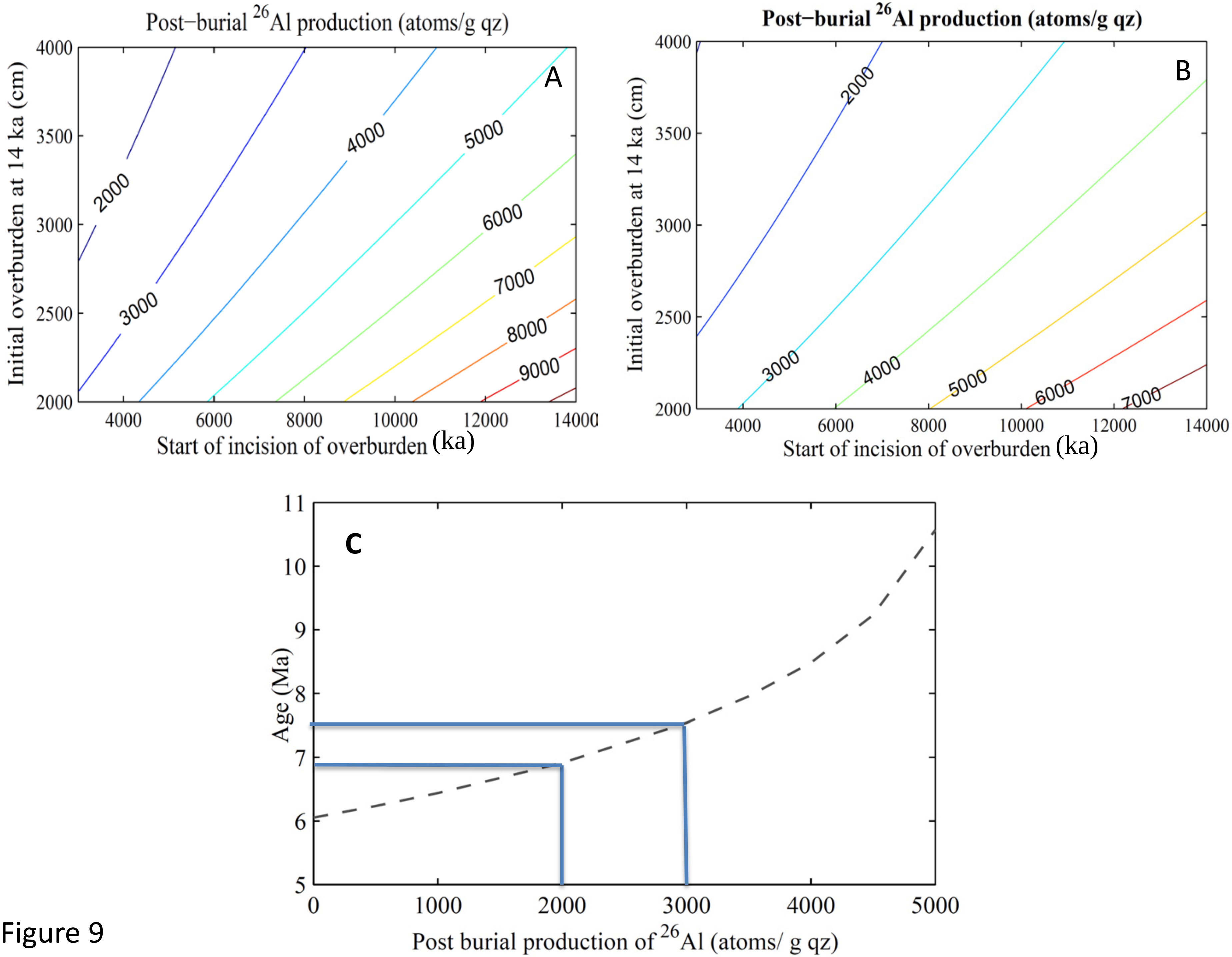

Post−burial ^{26}Al production (atoms/g qz)
A
Initial overburden at 14 ka (cm)
Start of incision of overburden (ka)
2000
3000
4000
5000
6000
7000
8000
9000
Post−burial ^{26}Al production (atoms/g qz)
B
Initial overburden at 14 ka (cm)
Start of incision of overburden (ka)
2000
3000
4000
5000
6000
7000
C
Age (Ma)
Post burial production of ^{26}Al (atoms/ g qz)

Figure 9